

SYNTHESES OF BENZOTRIAZOLE BASED CONJUGATED POLYMERS FOR
ORGANIC LIGHT EMITTING DIODE AND ORGANIC SOLAR CELL

A THESIS SUBMITTED TO
THE GRADUATE SCHOOL OF NATURAL AND APPLIED SCIENCES
OF
MIDDLE EAST TECHNICAL UNIVERSITY

BY

İPEK ÖNK

IN PARTIAL FULFILLMENT OF THE REQUIREMENTS
FOR
THE DEGREE OF MASTER OF SCIENCE
IN
POLYMER SCIENCE AND TECHNOLOGY

JUNE 2016

Approval of the thesis:

**SYNTHESES OF BENZOTRIAZOLE BASED CONJUGATED POLYMERS
FOR ORGANIC LIGHT EMITTING DIODE AND ORGANIC SOLAR CELL**

submitted by **İPEK ÖNK** in partial fulfillment of the requirements for the degree of
**Master of Science in Polymer Science and Technology Department, Middle East
Technical University** by,

Prof. Dr. Gülbin Dural Ünver
Dean, Graduate School of **Natural and Applied Sciences**

Prof. Dr. Necati Özkan
Head of Department, **Polymer Science and Technology**

Assoc. Prof. Dr. Ali Çırpan
Supervisor, **Polymer Science and Technology Dept., METU**

Assoc. Prof. Dr. Yasemin Arslan Udum
Co-Supervisor, **Advanced Technologies Dept., Gazi University**

Examining Committee Members:

Prof. Dr. Levent Toppare

Chemistry Dept., METU

Assoc. Prof. Dr. Ali Çırpan
Chemistry Dept., METU

Assoc. Prof. Dr. Yasemin Arslan Udum
Advanced Technologies Dept., Gazi University

Assoc. Prof. Dr. Gülay Ertuş
Chemistry Dept., METU

Asst. Prof. Dr. Görkem Günbaş
Chemistry Dept., METU

Date: 16.06.2016

I hereby declare that all information in this document has been obtained and presented in accordance with academic rules and ethical conduct. I also declare that, as required by these rules and conduct, I have fully cited and referenced all material and results that are not original to this work.

Name, Last name: İPEK ÖNK

Signature:

ABSTRACT

SYNTHESES OF BENZOTRIAZOLE BASED CONJUGATED POLYMERS FOR ORGANIC LIGHT EMITTING DIODE AND ORGANIC SOLAR CELL

Önk, İpek

M.S., Department of Polymer Science and Technology

Supervisor: Assoc. Prof. Dr. Ali Çırpan

Co-Supervisor: Assoc. Prof. Dr. Yasemin Arslan Udum

June 2016, 82 pages

Nowadays, people are on the edge of huge energy problem since the concentrations of greenhouse gases are dramatically increased and it causes the greenhouse effect that lead to warming of the Earth. In order to lessen the effect, OLED devices gain importance since they help to decrease the energy consumption because of its low driving voltage. Therefore, the discovery of OLED ushered a new epoch for flat panel displays and solid state lighting. The most powerful candidate of green energy source is the solar energy because electricity is generated by using sun light. In this manner, polymer light emitting diode and organic solar cell (OSC) devices were constructed. In this study, benzotriazole based conjugated polymers containing selenophene as π bridges were coupled with fluorene and carbazole via Suzuki condensation reaction. The structures of polymers were verified with NMR and molecular weights of polymers were determined via GPC. OLEDs with an ITO/PEDOT:PSS/polymer/LiF/Al configuration was constructed by using newly synthesized polymers and orange color was observed. Luminance values were determined as 6608 cd/m² for **P1** and 2540 cd/m² luminance for **P2**. Luminous efficiencies were 0.95 cd/A for **P1** at 8.0 V and 0.27 cd/A for **P2** at 9.5 V, respectively. Photovoltaic properties of **P2** were investigated using ITO/PEDOT:PSS/**P2**:PC₇₁BM/LiF/Al device configuration. The best performance of

P2 based OSC device showed a V_{oc} 0.86 V, a J_{sc} of 4.32 mA/cm², a fill factor (FF) of 47.0 %, and a PCE of 1.75% under standard AM 1.5 G at 100 mW/cm².

Keywords: Conjugated polymer, benzotriazole, selenophene, fluorene, carbazole, OLED

ÖZ

ORGANİK IŞIK YAYAN DİYOTLAR VE ORGANİK GÜNEŞ PİLLERİ İÇİN BENZOTRIAZOL İÇEREN KONJUGE POLİMERLERİN SENTEZİ

Önk, İpek

Yüksek Lisans, Polimer Bilim ve Teknolojisi Bölümü

Tez Yöneticisi: Doç. Dr. Ali Çırpan

Ortak Tez Yöneticisi: Doç. Dr. Yasemin Arslan Udum

Haziran 2016, 82 sayfa

Günümüzde, sera gazı konsantrasyonunun önemli ölçüde artmasından dolayı dünya ısınıyor ve insanlar büyük bir enerji probleminin eşiğindedir. Bu etkiyi azaltmak için, düşük çalışma voltajlarının enerji tüketiminin azalmasına yardım etmesinden dolayı, OLED cihazları önem kazanmıştır. Sonuç olarak, OLED'lerin keşfi düz panel ekran ve katı hal aydınlatmada yeni bir çağ açmıştır. Güneş enerjisi kullanılarak elektrik elde edilebildiğinden, yeşil enerji kaynaklarının en güçlü adayı güneş enerjisidir. Bu bağlamda, polimer ışık yayan diyot ve organik güneş pili cihazları yapılmıştır. Bu çalışmada, kimyasal yöntemle benzotriazol ünitesi içeren ve selenofenenin köprü bileşiği olarak kullanıldığı yeni polimerler Suzuki kenetlenme reaksiyonu ile sentezlenmiştir. Polimerlerin yapıları NMR ile belirlendi ve moleküler ağırlıkları GPC yöntemiyle incelendi. ITO/PEDOT: PSS/polimer/LiF/Al cihaz yapısına sahip yeni sentezlenmiş polimerlerle üretilmiş OLED'lerin karakteristik özellikleri belirlendi ve turuncu renk gözlemlendi. Luminans değerleri **P1** için 6608 cd/m² ve **P2** için 2540 cd/m² olarak belirlendi. Parlaklık verimi, **P1** için 8.0 V'da 0.95 cd/A ve **P2** için 9.5 V'da 0.27 cd/A olarak bulundu. **P2**'nin fotovoltik özellikleri ITO/PEDOT:PSS/**P2**:PC₇₁BM/LiF/Al yapısındaki cihaz kullanılarak incelendi. **P2** ile

yapılan organik güneş pili çalışmalarında en iyi performans AM 1.5 G aydınlatma (100 mW/cm²) altında V_{oc} değeri 0.86 V, J_{sc} değeri 4.32 mA/cm², doluluk oranı 47.0% ve PCE değeri 1.75% olarak bulundu.

Anahtar Kelimeler: Konjuge polimer, benzotriazol, selenofen, fluoren, karbazol, OLED

To my family

ACKNOWLEDGEMENTS

It is a gladness to thank many people who made the completion of this thesis possible. Foremost among them, I acknowledge my supervisor, Assoc. Prof. Dr. Ali ırpan for the opportunity to do a M.Sc., infinite guidance and patience.

I would like to thank Prof. Dr. Levent Toppare for his scientific support and expertise during my thesis study.

I would like to thank Assoc Prof. Dr. Yasemin Arslan Udum for her valuable support.

Thanks to Nima, Hande, Duygu, Aslı, zge, Soner, Ece, Cansel, Janset, Emre, Sultan and Fatma Demir for their help and friendly working environment.

Thanks to Őevki Can Cevher for his many useful comments on drafts of thesis study and endless sharing of their knowledge and experience with me.

Thanks to Őerife zdemir Hacıođlu for help in the electrochemical characterization and Gnl Hızalan for help in the OLED and solar cell characterization.

There have been many incredible people who shared the last few years with me. Among them are Yasemin DurmuŐ, Oya Gl, Zeren Tomruk, isem alıŐkan, Emre Erol, zge Azeri and of course Ahmet Gler. Thank you.

Lastly, I thank you to my parents for all the support, patience and favor.

TABLE OF CONTENTS

ABSTRACT	v
ÖZ	vii
ACKNOWLEDGEMENTS	x
TABLE OF CONTENTS	xi
LIST OF FIGURES	xiv
LIST OF TABLES	xvii
NOMENCLATURE	xviii
CHAPTERS	xx
1. INTRODUCTION	1
1.1. Historical Background	1
1.2. Conjugated Conducting Polymers	2
1.3. Band Gap Theory	3
1.4. Doping Process	5
1.5. Electrochromism in Conducting Polymers	7
1.6. Luminescence	9
1.6.1. Electroluminescence	10
1.6.2. Photoluminescence	11
1.7. Energy Transfer Mechanism	13
1.7.1. Förster Energy Transfer	13
1.7.2. Dexter Energy Transfer	14
1.8. Organic Light Emitting Diodes (OLEDs)	15
1.8.1. Basic Structure of OLEDs	17
1.8.2. Working Principle of OLEDs	18
1.9. Organic solar Cells (OSC)	19
1.9.1. Donor-Acceptor Approach	21

1.9.2. Basic Structure of OSC	23
1.9.3. Working Principle of OSC	24
1.9.4. OSC Characterization	25
1.10. Benzotriazole Based Conjugated Polymers.....	27
1.11. Aim of Thesis.....	30
2. EXPERIMENTAL	33
2.1. Materials and Equipments.....	33
2.2. Synthetic Procedure.....	34
2.2.1. Synthesis of 9-(bromomethyl) nonadecane.....	34
2.2.2. Synthesis of 4, 7-dibromobenzo[c] [1, 2, 5] thiadiazole	35
2.2.3. Synthesis of 3, 6-dibromobenzene-1, 2-diamine	35
2.2.4. Synthesis of 4, 7-dibromo-2H-benzo[d] [1, 2, 3] triazole.....	36
2.2.5. Synthesis of 4, 7- dibromo- 2- (2-octyldodecyl)-2H-benzo[d] [1, 2, 3] triazole.....	37
2.2.6. Synthesis of tributyl (selenophen-2-yl) stannane.....	37
2.2.7. Synthesis of 2-(2-octyldodecyl)-4, 7-di (selenophen-2-yl)-2H-benzo [d] [1, 2, 3] triazole	38
2.2.8. Synthesis of 4, 7-bis (5-bromoselenophen-2-yl)-2-(2-octyldodecyl)-2H-benzo[d][1,2,3]triazole	39
2.2.9. Synthesis of 4-(5-(7-methyl-9, 9-dioctyl-9H-fluoren-2-yl)-7-(5-methyl selenophen-2-yl)-2-(2-octyldodecyl)-2H-benzo[d] [1, 2, 3]triazole (P1).....	40
2.2.10. Synthesis of 9-(heptadecan-9-yl)-2-methyl-7-(5-(7-(5-methyl selenophen-2-yl)-2-(2-octyldodecyl)-2H-benzo[d][1,2,3]triazol-4-yl) selenophen – 2 -yl)-9H-carbazole (P2).....	41
2.3. Electrochemical Studies	42
2.4. Spectroelectrochemical Studies	43
2.5. Kinetic Studies	43
2.6. Gel Permeation Chromatography.....	44
2.7. OLED Studies.....	44
2.8. OSC Studies.....	45
3. RESULTS AND DISCUSSIONS	47
3.1. Electrochemical Properties	47

3.2. Optical Properties	49
3.3. Scan Rate Studies	52
3.4. Spectroelectrochemical Properties of Polymers	53
3.5. Kinetic Studies	55
3.6. OLED Applications	57
3.7. Solar Cell Applications	62
4. CONCLUSION	65
REFERENCES	67
APPENDICES	75
A. NMR DATA	75

LIST OF FIGURES

FIGURES

Figure 1. Common examples of conjugated polymer.....	3
Figure 2. Schematic view of a energy band gaps in metal (a), insulator (b) and semiconductor (c).....	5
Figure 3. Band models for trans- polyacetylene.....	7
Figure 4. Proposed structure of polypyrrole.....	7
Figure 5. The color change in neutral and oxidized states of polythiophene with small modifications in polymer backbone.....	8
Figure 6. Schematic view of photoluminescence.....	11
Figure 7. Schematic view of fluorescence.....	12
Figure 8. Schematic view of phosphorescence.....	13
Figure 9. Förster energy transfer mechanism.....	14
Figure 10. Dexter energy transfer mechanism.....	14
Figure 11. Schematic view of OLED device configuration.....	17
Figure 12. The working principle of OLED.....	19
Figure 13. Schematic view of donor-acceptor approach.....	23
Figure 14. Demonstration of OSC device configuration.....	24
Figure 15. Working principle of OSC.....	25
Figure 16. Current-voltage curve under dark and illumination.....	26
Figure 17. Some Literature Examples.....	28
Figure 18. Chemical structures of donor and acceptor groups.....	30
Figure 19. The molecular structures of synthesized polymers in this study.....	31
Figure 20. Synthesis of 9-(bromomethyl) nonadecane.....	34
Figure 21. Synthesis of 4, 7-dibromobenzo[c][1,2,5] thiadiazole.....	35
Figure 22. Synthesis of 3, 6-dibromobenzene-1, 2-diamine.....	35
Figure 23. Synthesis of 4, 7-dibromo-2H-benzo[d] [1,2,3] triazole.....	36
Figure 24. Synthesis of 4, 7- dibromo- 2- (2-octyldodecyl)-2H-benzo[d] [1,2,3] triazole.....	37
Figure 25. Synthesis of tributyl (selenophen-2-yl) stannane.....	37
Figure 26. Synthesis of 2-(2-octyldodecyl)-4, 7-di (selenophen-2-yl)-2H-benzo [d] [1,2 3] triazole.....	38
Figure 27. Synthesis of 4, 7-bis (5-bromoselenophen-2-yl)-2-(2-octyldodecyl)-2H-benzo[d][1,2,3] triazole (M1).....	39

Figure 28. Synthesis of 4-(5-(7-methyl-9, 9-dioctyl-9H-fluoren-2-yl)-7-(5-methyl selenophen-2-yl)-2-(2-octyldodecyl)-2H-benzo[d] [1,2,3] triazole (P1).....	40
Figure 29. Synthesis of 9-(heptadecan-9-yl)-2-methyl-7-(5-(7-(5-methyl selenophen-2-yl)-2-(2-octyldodecyl)-2H-benzo[d][1,2,3]triazol-4-yl) selenophen - 2 -yl)-9H-carbazole (P2).....	41
Figure 30. Single scan cyclic voltammograms of polymer films in 0.1 M TBAPF ₆ /ACN electrolyte solution (a) P1 (b) P2	48
Figure 31. Normalized absorption spectra of (a) P1 and (b) P2 in chloroform and in the thin film.....	51
Figure 32. The scan rates studies in 0.1 M TBAPF ₆ / ACN at scan rates of 100, 150, 200, 250 and 300mV/s for (a) P1 and (b) P2	53
Figure 33. Spectroelectrochemical graphs and colors of (a) P1 (b) P2 at various applied potential.....	55
Figure 34. Percent transmittance changes of (a) P1 and (b) P2 in 0.1 M TBAPF ₆ / ACN electrolyte solution at maximum wavelengths of polymers.....	56
Figure 35. The photoluminescence spectra of (a) P1 and (b) P2 in the thin film and in chloroform solution.....	58
Figure 36. The energy levels of materials used in OLED device fabrication.....	59
Figure 37. Current density-voltage-luminance characteristics of the (a) ITO/PEDOT:PSS/ P1 /LiF/Al device and (b) ITO/PEDOT:PSS/ P2 /LiF/Al device	60
Figure 38. Electroluminescence spectra of (a) ITO/PEDOT:PSS/ P1 /LiF/Al device and (b) ITO/PEDOT:PSS/ P2 /LiF/Al device.....	61
Figure 39. The CIE chromaticity diagram of ITO/PEDOT:PSS/polymers/LiF/Al...	61
Figure 40. Photographs of an OLED device containing (a) P1 and (b) P2	62
Figure 41. The energy levels of materials used in OSC device fabrication.....	62
Figure 42. Light <i>J-V</i> characterization of the polymer solar cells made from P2 blended with PC ₇₁ BM.....	63
Figure 43. IPCE curve of photovoltaic device using P2 donor blended with PC ₇₁ BM.....	64
Figure 44. ¹ H NMR of 9-(bromomethyl) nonadecane.....	75
Figure 45. ¹³ C NMR 9-(bromomethyl) nonadecane.....	76
Figure 46. ¹ H NMR of tributyl(selenophen-2-yl)stannane.....	76
Figure 47. ¹³ C NMR of tributyl(selenophen-2-yl)stannane.....	77
Figure 48. ¹ H NMR of 4, 7-dibromobenzo[c][1,2,5]thiadiazole.....	77
Figure 49. ¹³ C NMR of 4, 7-dibromobenzo[c][1,2,5] thiadiazole.....	78
Figure 50. ¹ H NMR of 4, 7-dibromo-2H-benzo[d][1,2,3]triazole.....	78
Figure 51. ¹ H NMR of 4, 7-dibromo-2-(2-octyldodecyl) - 2H -benzo[d] [1, 2, 3] triazole.....	79
Figure 52. ¹³ C MNR of 4, 7-dibromo-2-(2-octyldodecyl) - 2H -benzo[d] [1, 2, 3] triazole.....	79

Figure 53. ¹ H NMR of 2-(2-octyldodecyl)-4, 7-di (selenophen-2-yl)-2 H benzo [d] [1, 2, 3] triazole.....	80
Figure 54. ¹³ C NMR of 2-(2-octyldodecyl)-4, 7-di (selenophen-2-yl)-2 H benzo [d] [1, 2, 3] triazole.....	80
Figure 55. ¹ H NMR of 4, 7-bis (5-bromoselenophen-2-yl)-2-(2-octyldodecyl)-2Hbenzo[d][1,2,3]triazole.....	81
Figure 56. ¹³ C NMR of 4, 7-bis (5-bromoselenophen-2-yl)-2-(2-octyldodecyl)-2Hbenzo[d][1,2,3]triazole.....	81
Figure 57. ¹ H NMR of P1	82
Figure 58. ¹ H NMR of P2	82

LIST OF TABLES

TABLES

Table 1. Brief information about types of luminescence	10
Table 2. The basic results of the studied polymers in literature	29
Table 3. Summary of electrochemical studies	49
Table 4. Results of absorption spectra of P1 and P2 in chloroform and thin film	50
Table 5. Optical contrast and switching time values of P1 and P2	57
Table 6. The result of OSC device	64

NOMENCLATURE

AM 1.5G	Air mass 1.5 global
ACN	Acetonitrile
BHJ	Bulk heterojunction
BTz	Benzotriazole
CB	Conduction band
CE	Counter electrode
CP	Conjugated polymer
CV	Cyclic voltammetry
D/A	Donor-Acceptor
EC	Electrochromic
EL	Electroluminescence
ETL	Electron transport layer
EQE	External quantum efficiency
FRET	Fluorescence resonance energy transfer
HOMO	Highest occupied molecular orbital
HTL	Hole transport layer
GPC	Gel permeation chromatography
ICT	Intermolecular charge transfer
IPCE	Internal power conversion efficiency

ITO	Indium tin oxide
LED	Light emitting diode
LUMO	Lowest unoccupied molecular orbital
NIR	Near infrared
OLED	Organic light emitting diode
OSC	Organic solar cell
PC ₇₁ BM	[6,6]-Phenyl C 71 butyric acid methyl ester
PCE	Power conversion efficiency
PEDOT	Polyethylene dioxythiophene
PL	Photoluminescence
PSS	Polystyrene sulfonate
P-OLED	Polymer based organic light emitting diode
RE	Reference electrode
SHE	Standard hydrogen electrode
S-OLED	Small molecule organic light emitting diode
THF	Tetrahydrofuran
TBAPF ₆	Tetrabutylammonium hexafluorophosphate
UV	Ultraviolet
VB	Valence band
WE	Working electrode
Vis	Visible

η_e	Power conversion efficiency
J_{sc}	Short circuit current density
V_{oc}	Open circuit voltage
FF	Fill factor
P_{max}	Maximum power
P_{in}	Power of the incident light
Eg^{op}	Optical band gap
Eg^{el}	Electronic band gap

CHAPTER 1

INTRODUCTION

1.1. Historical Background

Exploration of electroluminescence (EL) phenomenon takes place thanks to carborundum (SiC) crystal found by H.J. Round in early 1907 and this progress push ahead with discovery of inorganic light emitting diodes in 1962 by Nick Holonyak Jr. [1]. Commercially production of first LEDs based on gallium arsenide phosphide (GaAsP) date to 1968. Then, Bernanose applied a high voltage alternating current to acridine orange and quinacrine films and hereby first organic EL was invented. Afterwards, Pope and his team observed direct current electroluminescence by using pure crystal of anthracene which is an organic semiconductor. Pope claimed that recombination of electrons and holes occur due to electroluminescence. The recombination of electrons and holes are known as excitons. Moreover, in 1963, anthracene crystals doped via tetracene. In early 1975, first organic electroluminescence device was performed by using a polymer polyvinyl carbazole (PVK) [2].

In early days of organic EL, the driving voltage was higher than 100 V to obtain sufficient light output [3]. Later, the academic research of Tang was financially supported by Kodak Chemical demonstrated the first efficient organic light emitting

diode (OLED) devices by using multilayer configuration. They deposited thin film of anthracene thermally and this reduced the operating voltage under 30 V. In 1990, Burroughes improved a green light emitting polymer device by using poly (p-phenylene vinylene) which is more efficient than poly (n-vinylcarbazole). After this development, small molecule organic light emitting diodes (SMOLEDs) have been deposited thermally and still by using this method SMOLEDs such as smart phones, tablets, CD/MP3 players, automobile audio systems, digital camera and etc. have been produced commercially [4]. After the invention of photovoltaic effect in 1839, first selenium based solar cell was discovered in 1883 [5,6]. In 1954, first solar cells with silicon doped were developed [7]. The first solar panels were fabricated in 1976s [8].

The discovery and development of conjugated polymers in 1977 brought Alan J. Heeger, Alan G. MacDiarmid, and Hideki Shirakawa Nobel prize in 2000 [9]. They proved that the conjugated polymers are electrically conductive with doping [10]. After the discovery of conjugated polymers, academic and industrial researches have been increased day after day.

1.2. Conjugated Conducting Polymers

Basically, conjugated polymers are macromolecules and electrons can be delocalized through the polymer backbone in which single and double or single and triple bonds alternate. Hence, they can gain some amazing qualifications like high conductivity and fascinating optical and electrical qualities [11]. Owing to flexibility, corrosion resistant and processability in addition to their optical and electrical qualities, they can be utilized in numerous areas such as polymer light emitting diodes [12], organic thin film transistors (OTFTs) [13], sensors [14] and solar cells [15].

Along the metal structure, electrons can move freely and this property makes the metals conductive. By analogy, to make the polymers electronically conductive, the polymers have both charge carriers and suitable orbital system that maintains the movement of charge carriers [11]. The energy difference between the highest

occupied molecular π orbital and the lowest unoccupied molecular π^* orbital is named as band gap. For semiconductors, the ideal band gap is between from 1.5 to 3.0 eV. If the perfect conducting polymer is imagined, its electrons should be delocalized along the whole chain thanks to π conjugation. But in reality, the polymer chain may have some intrinsic and external defects. External impurities may be derived from the existence of O, Cl, and F atoms since they can eliminate the double bond. On the other hand, torsional conformations or crosslink formation via neighboring may cause intrinsic defects because they can break the conjugation. Generally, the polymer film has between from 5 to 15 repeating units. Band gap reduces with rising conjugation length [16]. The structures of common conjugated polymers are depicted in Figure 1.

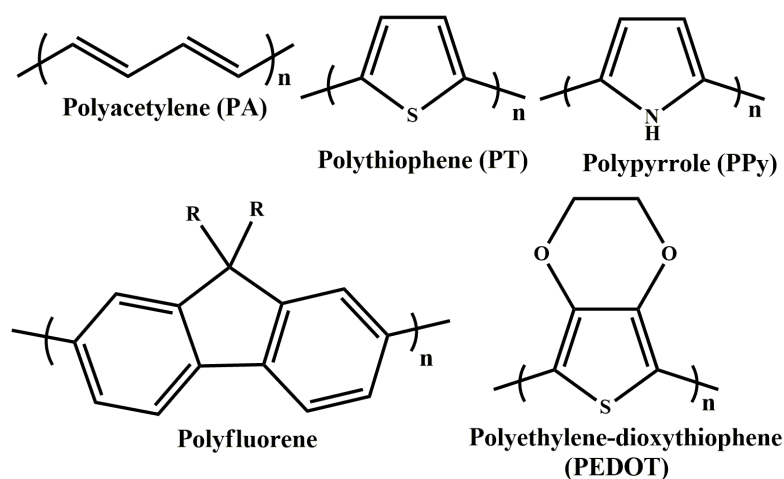


Figure 1. Common examples of conjugated polymer

1.3. Band Gap Theory

In 1979, Harrison states band theory for inorganic semiconductors. This theory mentions that the electrical properties of band gap can be defined by using the discrete energy states (bands) where the movements of electrons occur. Likewise, fully occupied π band and empty π^* band are created by the π electron materials for organic semiconductors [11].

Valence band (VB) is the occupied band by electrons whereas conduction band (CB) includes unfilled band above the VB at 0 K in semiconductors. Electrical conductivity is directly related to amount of electrons in materials. Metals are known as having high conductivity due to a great number of electrons attends to carriage of current. Because of this, it is hard to change the conductivity of metal. On the other hand, semiconductors are assumed having no conductivity at 0 K and very low conductivity at measurable temperatures. Thus, the conductivity of semiconductor can be changed at wide temperature range and this feature makes the semiconductors powerful candidate for optoelectronic devices [17].

In other words, while the highest occupied band is named as VB, the lowest unoccupied band is named as CB. Band gap is the energy difference between conduction and valence bands. Furthermore, materials can be classified as metals, insulators, and semiconductors according to different electrical conduction properties that are indicated in Figure 2. First of all, metals have not band gap (E_g) between valence and conduction band. In other words, these two bands are overlapped so they are highly conductive materials. Secondly, insulators have high energy gap between fully occupied VB and fully empty CB. Thus, there is not any electrical conductivity since electron movement does not occur. Lastly, conjugated polymers are different than other organic materials and other kind of polymers. Since conducting polymers include many π and π^* energy levels, this makes the band gap low compare to those of insulators. Thus, semiconductors have narrower band gap than insulators and when additional energy is given, an electron can be moved from VB to CB [11].

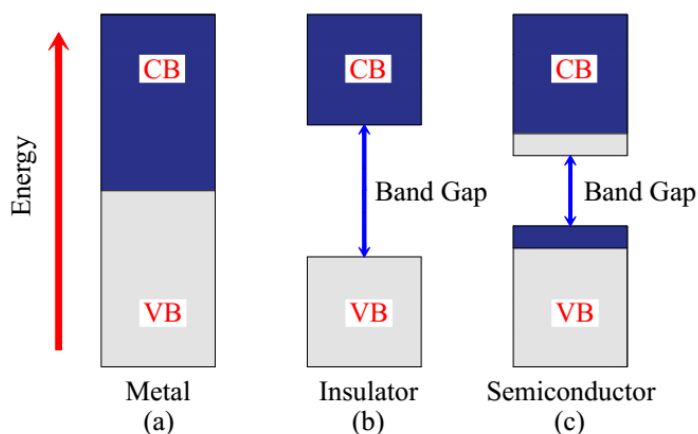


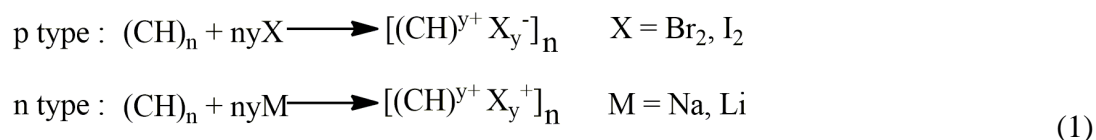
Figure 2. Schematic view of a energy band gaps in metal (a), insulator (b) and semiconductor (c)

1.4. Doping Process

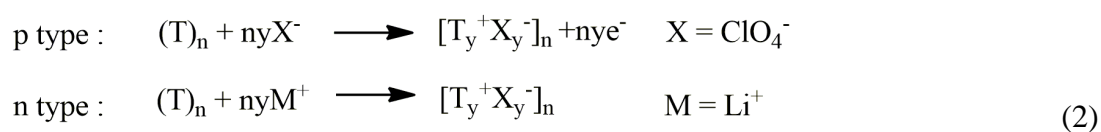
Conjugated polymers are insulators in their ground state. In order to acquire electrical conductivity qualification, doping process should be applied to obtain free charges. Since there is a narrower band gap for conjugated polymers, the band gap can be altered by extracting electrons from the valence band (HOMO) or donating electrons to the conduction band (LUMO). This process is reversible and existence of charge carriers is one of the main requirements for providing conductivity. With this notion, partial oxidation (p dope) by using electron acceptors (e.g. I_2 , AsF_5) or partial reduction (n dope) by using electron donors (e.g. Na, K) can be applied in order to produce accessional charge carriers. As a result, positively charged cations and negatively charged anions are formed. These forming charges are neutralized by dopants. During the doping process, charge defects whose names are polaron, bipolaron and soliton have been created [18].

Doping process can be done by using chemical or electrochemical way. During chemical doping, a polymer reacts with oxidizing or reducing reagent. Similarly, polymer film is oxidized or reduced in solution with suitable voltage during electrochemical doping [19].

In the past, doping was done chemically by using oxidizing agents (e.g. iodine sublimation or hot bromine gas) or small atoms (e.g. lithium, cesium). But these methods cause instability in device due to diffusion of anions/cations. Related chemical mechanism of chemical doping of polyacetylene is indicated in equation 1 [20].



Later on, electrochemical doping is used a better alternative due to its numerous advantages. Related chemical equation of electrochemical doping of polythiophene is depicted in equation 2. First of all, intended doping level can be obtained by managing the current passed. The other advantage is that there is a considerable reversible doping dedoping process without removal of any side products. During doping process, degradation should not occur to remain main structure of the polymer. It is the one of the main requirements of the electrochemical polymerization in order to utilize polymers for an electrochromic application [20].



As mentioned before, during redox reactions, there is an electron exchange and it causes formation of solitons, polarons and bipolarons. Degenerate ground state molecules are denominated as by solitons and they are similar to polyacetylene form. Non degenerate ground states (heterocyclic compounds) are known as polarons and bipolarons. Free radicals are formed through the polymerization of polyacetylene and they are known as soliton. Depend on redox process, solitons can be charged positively or negatively [20]. It is depicted in Figure 3.

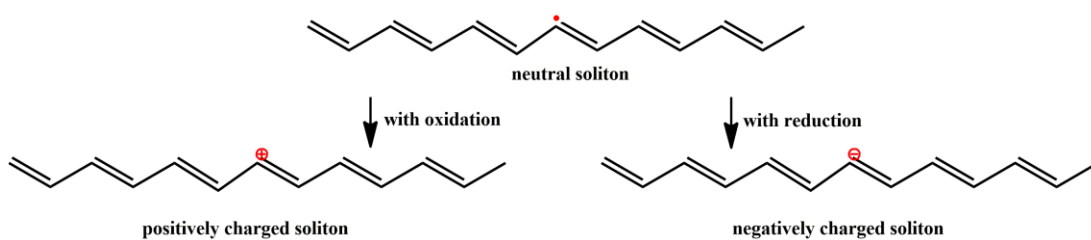


Figure 3. Band models for trans- polyacetylene

On the other hand, radical anions or cations are formed through the polymerization of heterocyclic compounds thanks to the ionization of polymers and they are called as polarons. Moreover, bipolaron formation is also possible [21]. Related figure is indicated in Figure 4.

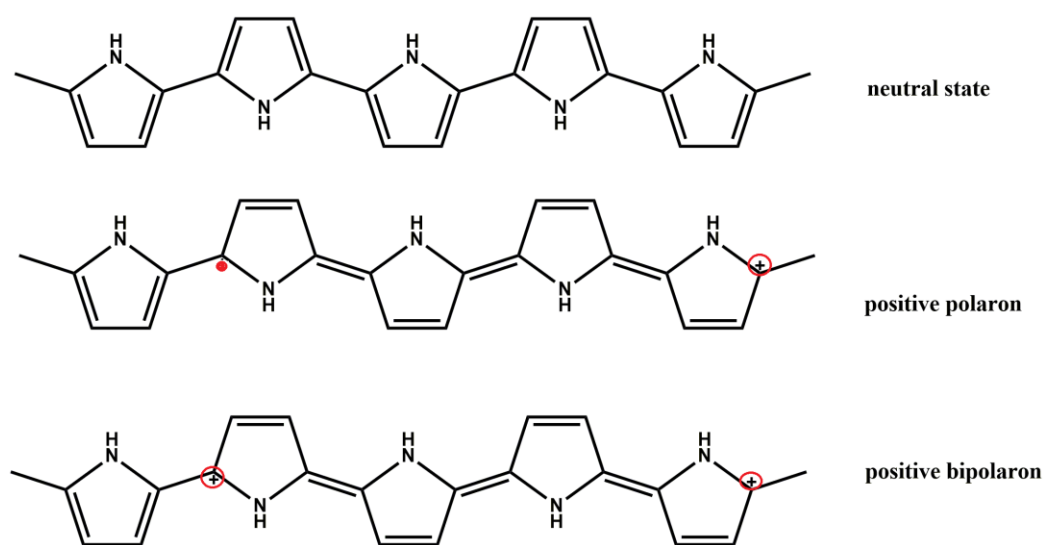


Figure 4. Proposed structure of polypyrrole

1.5. Electrochromism in Conducting Polymers

When appropriate electrode potential is applied, some polymers undergo temporary color change. This reversible optical change is called as electrochromism. Conjugated polymers are processable and they have fast response times, long lifetimes and high optical contrast so CP's can be used in electrochromic (EC) display technology. Range of application areas of EC materials is wide such as smart

windows, optical shutters and mirror devices for automobile industry. EC materials can be classified into three main groups according to electronically reachable optical states. Firstly, there are at least one colored and one transparent material. Metal oxides, viologens and polymer like poly (3, 4-ethylenedioxythiophene) (PEDOT), and the polynuclear transition metal hexacyanometallates are belong to first type EC materials (prussian blue electrochromism) and they can be applied as smart windows, information displays and optical shutters. Secondly, there are electrochromes that have two different colored states. Although they have not transmissive state, they are suitable for display applications since they show different colors during redox reaction. Polythiophene can be given as an example because its thin films indicate red color, and during oxidation it turns to blue. Lastly, there are at least two color states during different redox states. Blends and copolymers can be used as the third type EC materials and they are named as multichromic materials such as poly (3,4-propylenedioxyppyrole) [22]. The color change is indicated in Figure 5 in neutral and oxidized state as an example.

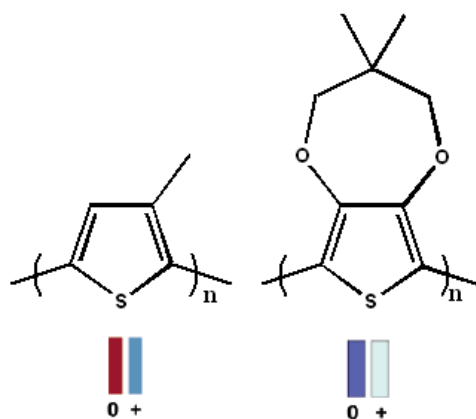


Figure 5. The color change in neutral and oxidized states of polythiophene with small modifications in polymer backbone

Practically, it is easy to evaluate electrochromism quantitatively using electrochromic contrast, switching speed, stability and optical memory, coloration efficiency [22]. Electrochromic contrast is crucial to interpret EC materials. Generally, it is depicted as percent transmittance change ($\Delta T \%$) at a particular

wavelength. This wavelength is determined by the material's maximum optical contrast. Switching speed defines the time needed for the coloring/transparent processes for EC materials. The material should be neutral during measurement. In other words, if the material is chemically stable (no oxidation or reduction), switching time is higher. This value is significant for dynamic displays and alterable mirrors. Ionic conductivity of the electrolyte, transportability of the ions to the electroactive sites, the amount of given potential, thickness and morphology of the film affect the switching speed. During redox reaction degradation occurs and it leads to decrease electrochromic contrast and hence EC material's performance decreases. Given excess potentials, side reactions due to the moisture in the cell and heat discharge because resistive component may cause reduction of the stability of EC's material. Optical memory can be identified as how much time passed during absorption state after the removal of the electric field. Coloration or EC efficiency detects the amount of optical density (ΔOD) excited as a function of the added or removed electronic charge (Q_d). In other words, the required amount of charge is determined to generate the optical change [22]. It is depicted by the equation 3.

$$\eta = (\Delta OD)/Q_d = \log[T_b/T_c]/Q_d \quad (3)$$

Where η ($\text{cm}^2 \text{C}^{-1}$): the coloration efficiency at a given λ

T_b : bleached transmittance value

T_c : colored transmittance value

Q_d : added or removed electronic charge [22].

1.6. Luminescence

Basically, there are two ways to create light which are incandescence and luminescence. Both are based on emission of light from a source. While incandescence is the emission of light from a hot body, luminescence is the emission of light from cold bodies. So, luminescence is also known as cold emission since emission of light can take place at normal and lower temperatures. In other words,

luminescence is the best alternative to generate light at ambient temperatures. Depending on different excitation sources, luminescence can take different names such as photoluminescence, electroluminescence, chemiluminescence and etc. that are shown at Table 1 [23].

Table 1. Brief information about types of luminescence

Source	Type of luminescence
Photons	Photoluminescence
Chemical reaction energy	Chemiluminescence
Electric field	Electroluminescence
Electrons	Catholuminescence

When a material is converted to ground state from excited state, an amount of energy is released. Thus, it causes the emission of light. In order to reach that excited state, photoexcitation (photoluminescence) or electronic excitation (electroluminescence) can be used [23].

1.6.1. Electroluminescence

Electroluminescence can be defined as the emission of light from a material by using electric field. In other words, after the excitation of material by electric current, a photon starts to decay to a lower energy state and the light generation can be observed. By using electroluminescence, high efficient illuminants can be obtained by using low driving voltages. If the semiconducting compound is doped, p-n junction occurs. It means that there is a recombination of electrons and holes. Then, a photon releases and this process is observed by a specific color [24]. Organic electroluminescence leads to light emission due to excitation of electrons from organic material. During organic electroluminescence, while electrons move to the LUMO level of the polymer from the cathode, electrons move to the HOMO level of the polymer from anode. Thus, electrons and holes are formed. The movement of electrons and holes depends on hopping mechanism. Since the electrons merge with holes in emissive compound, molecular excited states (excitons) are formed. Lastly,

the emissive compound becomes to release photons and they decay to generate light [23].

1.6.2. Photoluminescence

During photoluminescence, an electron is excited from HOMO to the LUMO thanks to incident photon. Then, these excitations become to relax via radiative or non radiative decay to the HOMO level from the LUMO level. If there is a radiative relaxation, this process is called as PL and a schematic of PL is depicted in Figure 6 [25].

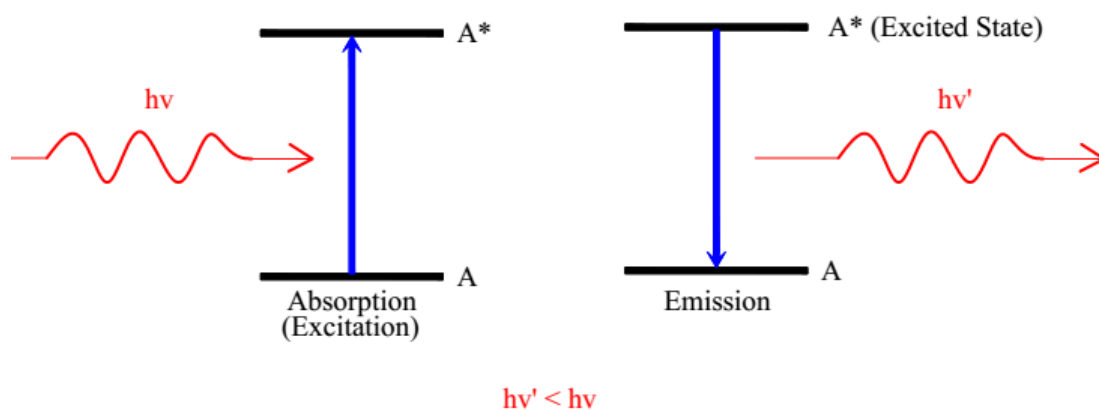


Figure 6. Schematic view of photoluminescence

1.6.2.1. Fluorescence

When excited material returns to the ground state from the excited singlet state via photon emission, it is called as fluorescence (Figure 7). Fluorescence has short life time and spin allowed transitions (by Pauli's exclusion principle) occur. Pauli Exclusion Principle mentions that the same quantum state cannot be taken up by two identical fermions (particles including half integer spin) concurrently. In other words, paired electron's spin is allowed during releasing an electron from singlet state whereas unpaired electron's spin is not allowed during decaying from triplet state [26].

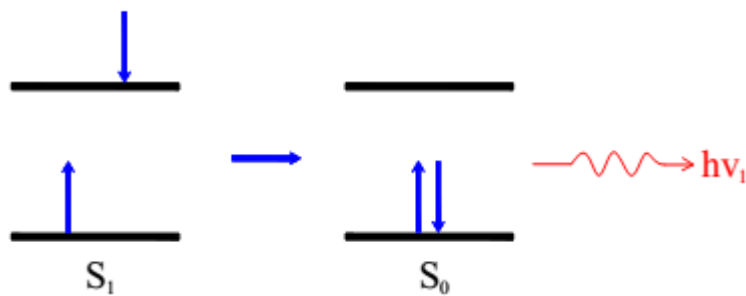


Figure 7. Schematic view of fluorescence

1.6.2.2. Phosphorescence

Like fluorescence, phosphorescence occurs when excited material comes back to the ground state by photon emission which is indicated in Figure 8. However, here, it happens from the excited triplet state. Moreover, while the radiative transition occurs between same multiplicities, for fluorescence it takes place between different multiplicities states. Phosphorescence has longer life time (1 sec) than fluorescence (10^{-9} sec) and there is a spin forbidden transition. Since longer life time is needed for phosphorescent transitions, the probability of carry of the radiationless transfer of energy increases. Hence, it usually happens at low temperatures or in rigid media. During phosphorescence, non radiative intersystem crossing (from S_1 to T_1) occurs by the spin orbit coupling. By using intersystem crossing (ISC), triplet state gains moderately singlet property and it makes the transition to the ground state possible. During photon emission, electrons transport to the lower energy states and it makes the band gap decrease. Thus, a longer wavelength is observed for emitted photon according to Planck-Einstein relation ($E=h\nu$ where E is the energy of photon, h is the Plank constant and ν is the frequency). Moreover, triplet excitons have lower energy than singlet excitons because of decreased repulsion [27].

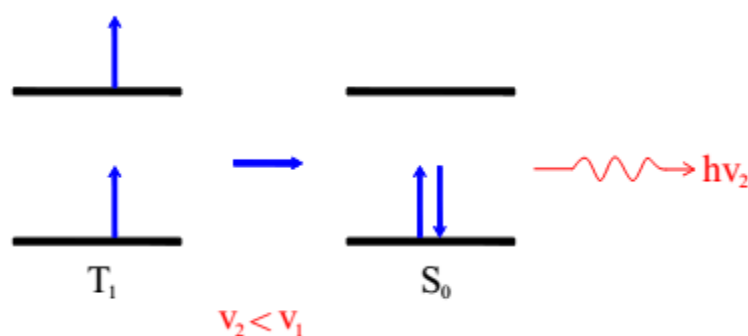


Figure 8. Schematic view of phosphorescence

1.7. Energy Transfer Mechanism

The first relaxation type is photon emission due to radiative decay and this subject is mentioned in section 1.6. Another way of relaxation is energy transfer mechanisms for excited molecules. Here, excitation energy is transformed through thermal processes like vibrational relaxation and collisional quenching instead of forming photons [28]. While the donor is still in the ground energy state, the acceptor is found in the excited energy state due to energy transfer [29]. If donor molecules have high band gap, composed excitons move to the acceptor molecule since acceptor molecules have lower band gap than donors. This transfer can be done by using Förster energy transfer of singlet excitons or Dexter energy exchange of triplet excitons [30].

1.7.1. Förster Energy Transfer

Förster Energy Transfer is used to investigate the excitons formation and its practicability. It is also known as Fluorescence Resonance Energy Transfer (FRET) [31]. Related mechanism is depicted in Figure 9. It occurs during participation of singlet excitons. During FRET, absorbed energy of donor is transferred to the lower band gap acceptor via non radiative energy transfer. In other words, excitation energy is carried on the acceptor from donor. After the recombination of charges, the acceptor emits the light. Förster energy transfer mechanism depends on energy transfer rate and long range dipole-dipole interaction. Emission spectrum of the

donor and absorption spectra of acceptor should overlap and if the distance between emission of donor and absorption of acceptor is higher than 10 nm, energy transfer is not observed. Moreover, uniform mixing is needed for effective FRET [32].

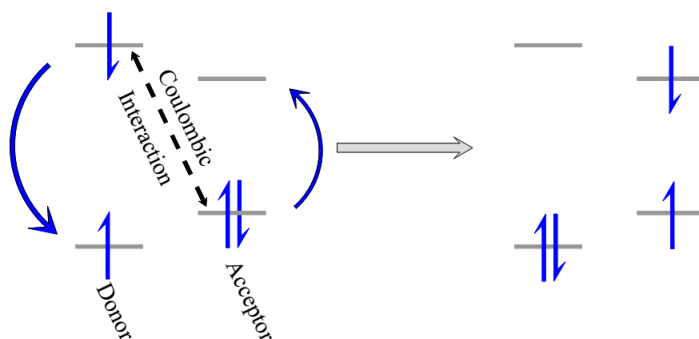


Figure 9. Förster energy transfer mechanism

1.7.2. Dexter Energy Transfer

During Dexter Energy Transfer, electrons are exchanged between donor and acceptors [33]. Necessary distance is less for effective Dexter energy transfer. Singlet- singlet and triplet-triplet transfers are allowed. It is usually observed for triplet emitters with metal complexes such as iridium complexes [34]. Related Dexter energy transfer mechanism is depicted in Figure 10.

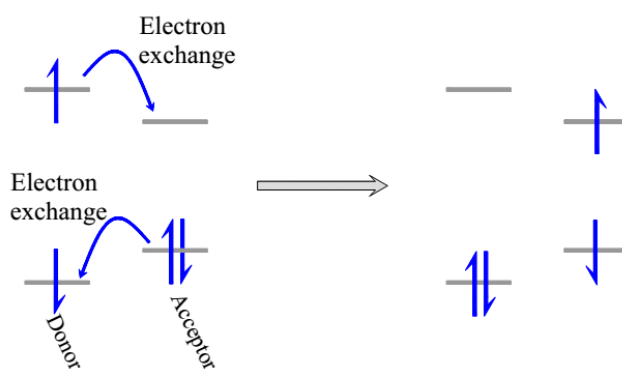


Figure 10. Dexter energy transfer mechanism

1.8. Organic Light Emitting Diodes (OLEDs)

In these days, concentrations of greenhouse gases are dramatically increased and it causes the greenhouse effect that lead to warming of the Earth. In order to lessen the effect, OLED devices gain importance since they help to decrease the energy consumption because of its low driving voltage. For OLED devices, low driving voltage is directly related to less heat generation. With this aim, the discovery of OLED ushered in a new epoch for flat panel displays and solid state lighting [35].

Today, tungsten filament bulbs are generally used for ambient lighting. They can convert approximately 10 % energy as light; the remaining is converted as heat. So, it causes poor efficiency. Alternatively, fluorescent light bulbs have started to be used since they have higher efficiency than tungsten filament bulbs. Moreover, their life time is approximately three times higher than tungsten filament bulbs. On the other hand, fluorescent light bulbs include mercury that is harmful for environment. Thus, integrating the lighting with OLED should be apt choice since OLEDs have already more efficient and higher greater lifer times than fluorescent bulbs [23].

At present, dominant solid display technology consists of inorganic light emitting diodes (LEDs). However, the developments of OLED technology have been increased exponentially in both academia and commerce. Thus, it is replace the inorganic LED technology due to their ease of fabrication, flexibility, transparency and low cost properties [36].

There are differences between organic and inorganic semiconductors. Firstly, organic semiconductors are conjugated organic compounds and there is a weak van der Waals interaction. On the other hand, inorganic ones have strong covalent bonds. Thus, organic semiconductors carry out weak intermolecular coupling and mobility of charge carriers are lower than inorganic ones. Moreover, hopping transport occurs for organic semiconductors but band transport performs for inorganic one. Dielectric constant for organic semiconductors (3-5 eV) is lower than inorganic ones (10-15 eV) [35].

Advantages of organic semiconductors are as follows [37];

- Light weight
- Mechanically flexible
- Ultra thin
- Cheaper processing (e.g. spin coating)
- Easy to chemical modifications
- Potential for future growth
- Low processing temperature: Processing temperature is usually lower than 100°C. Thus, plastic substrates can be used as substrate without degradation like glass substrate.

Disadvantages of OLEDs are the following [27];

- Not moisture resistant: OLED devices are sensitive to moisture and it causes degradation. However, encapsulation can be applied in order to get longer lifespan.
- Not UV resistant: OLED devices can degrade through UV exposure.

1.8.1. Basic Structure of OLEDs

OLED structure includes many layer that are depicted in Figure 11 [38].

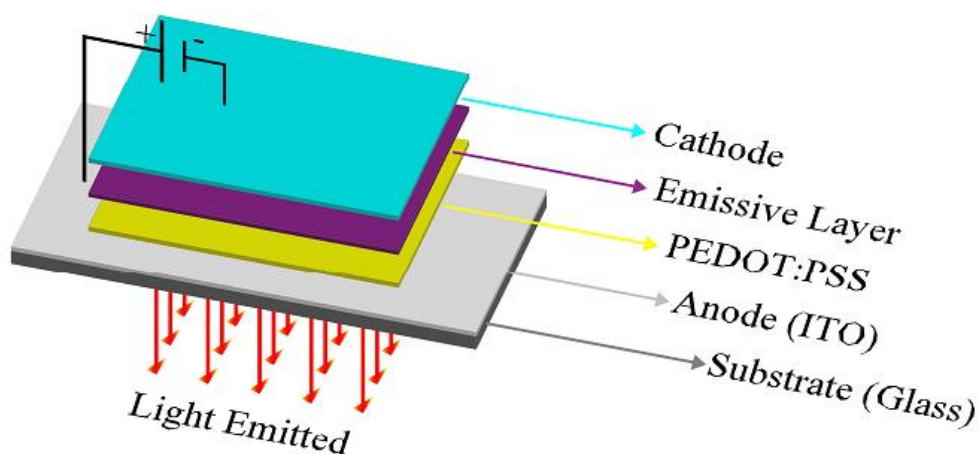


Figure 11. Schematic view of OLED device configuration

Substrates such as glass or transparent plastics are utilized in order to support the OLED device.

Anode materials are one of the basic requirements to inject holes during voltage application. They are coated over the substrate and they should be also transparent to see colors clearly. Furthermore, they should have some requirements in order to use a material as an anode [27]. First necessary is high work function since they help to hole injection to the emissive layer. Secondly, high conductivity is needed to minimize the contact resistance. In order to provide great contact to neighbor organic layers, they should have great film forming ability and wettability. High thermal and chemical stability supplies wide working range [39]. With this aim, generally indium tin oxide (ITO) is used as an anode since it has high transparency, good conductivity, favorable work function value and low resistivity [40].

Hole injection layer takes part between the anode and the emission layer. Poly (4-styrenesulfonate)-doped poly (3, 4-ethylenedioxythiophene) (PEDOT:PSS) is used as the hole injection layer. It is coated with spin coater and its thickness is generally

adjusted as 40 nm. PEDOT:PSS brings two main advantages in an OLED device. Firstly, it helps transportation of holes since HOMO energy level of PEDOT:PSS is coherent with the work function of ITO and HOMO level of emissive layer. Secondly, it provides good film coating ability to emissive layer by flattening the ITO surface [41].

Like anode materials, cathode materials should have some requirements in order to decrease the energy barrier between the electrode and emissive layer [42]. First requirement is low work function since they help electron injection to the emissive layer. Similar to anode materials, high conductivity, great film forming ability, wettability, high thermal and chemical stability are needed. With this aim, generally, pure metals like Ca, Mg, Al or their alloys are preferred. As mentioned before, cathode materials have lower work function than anode materials and the value is very close to the vacuum level. This property makes the cathode material unstable to air [43].

Fabrication of emissive layers can be classified as two main classes. First one is the thermal vacuum evaporation for small molecule OLEDs and second one is spin coating technique for PLEDs. In using spin coating technique, there are some important parameters such as concentration of polymer, spin rate and spin coating temperature in order to manage the thickness of polymer. If thermal vacuum evaporation technique is applied, thickness of layer is controlled easily. However, polymers cannot be coated by using thermal vacuum evaporation since polymers decompose during heating [44].

1.8.2. Working Principle of OLEDs

Basically, OLED structure consists of metal as cathode, emissive layer and ITO as anode. The selection of anode and cathode materials is important in order to provide transportation of charge carriers. Injection barrier is very crucial between Al and LUMO level of emissive layer and also between ITO and HOMO level of emissive layer. If the injection barrier is huge, there is no current. Since the difference between

Al and LUMO level of emissive layer is higher than ITO and HOMO level of emissive layer, injection of the electrons to the LUMO level of the polymer is hard. In other words, holes are close to the metal side so they can move faster.

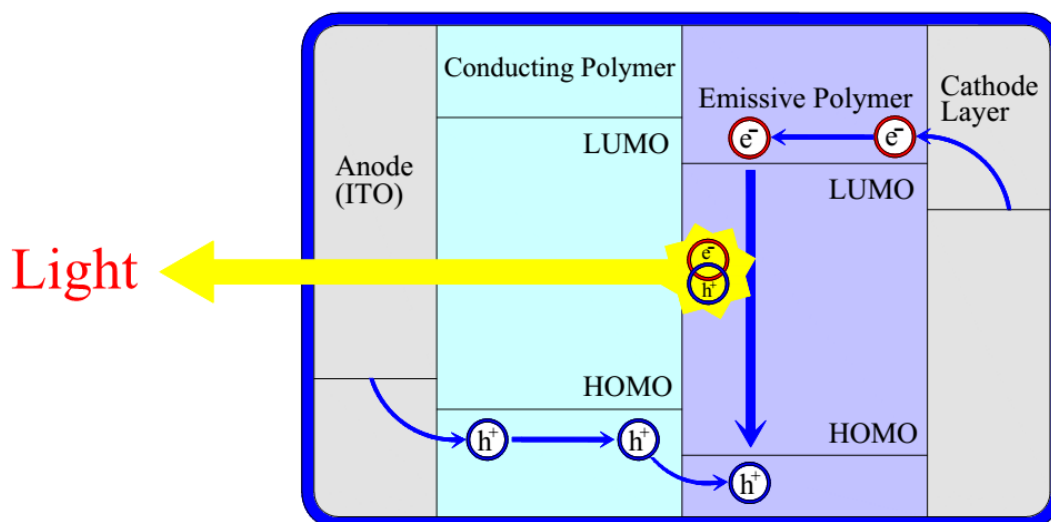


Figure 12. The working principle of OLED

OLED operation principle consists of 4 stages which is depicted in Figure 12 [45];

1. Electrons are injected from cathode to the LUMO level of the emissive layer. Similarly, holes are injected from anode to the HOMO level of the emissive layer.
2. Transportation of charge carriers occurs close to the emissive layer.
3. Charge recombination happens and it leads to the formation of excitons.
4. Decay of excitons occurs and light is emitted.

1.9. Organic solar Cells (OSC)

Today, people are on the edge of huge energy problem since generally fuels are consumed in order to get energy requirement. Fuels are finite sources and they release CO_2 gases. This causes the acceleration of global warming. The Intergovernmental Panel on Climate Change anticipated an increment of between 1.8°C and 4.0°C until the end of this century [46]. Sudden changes of average

temperature, tropical storms, drought and rising of sea level can be clearly observed as a result of climate changes. Some precautions can be taken to prevent harmful effects of climate change. Moreover, there will be a 60% rise in world's energy requirement up to 2030 [47]. With this aim, both clean and renewable sources are deliberated. Solar energy is one of the powerful candidates because of its theoretical potential. Solar energy is clean production since it does not emit CO₂ gases and other pollutant. Moreover, it is renewable since it is not a form of substance which is exists before hundreds of millions.

Organic solar cells (OSC) can be classified as single layer OSC, bilayer OSC and bulk heterojunction OSC. For organic solar cells, thickness of layer, excitons diffusion length and morphology affect the efficiency of OSC. Electric field is not enough for both single layer and bilayer OSC. Moreover, they have bad configuration for charge transfer. Thus, they have lower efficiencies than bulk heterojunction OSC. As a result, bulk heterojunction solar cells were preferred. One of the main advantages of bulk heterojunction OSC is they have controllable domain sizes. Domain size should be in the range of diffusion length. They enhance exciton diffusion energy since they reduce average distance for excitons require to travel to be dissociated. Diffusion length (LD) equation is depicted in equation 4. Diffusion coefficient indicates excition's diffusion rate within material or can hopping from molecule to molecule or chain to chain [48]. Higher D represents longer lifetime of excitons. Higher LD is preferable since higher LD increases the probability of reaching the D/A interface through its lifespan. If excitons cannot reach the D/A interface, excitons go to the ground state again and no electric generation is observed [49].

$$LD = \sqrt{D \tau} \quad (4)$$

Where LD is diffusion length

D is the diffusion coefficient

τ is the lifetime of exciton

Despite expensive fabrication costs, efficiencies of commercially available silicon based inorganic solar cells reached to 15% [50]. OSCs have affordable fabrication costs in comparison with inorganic ones. Moreover, thin films are used at low process temperature for OSC application and it also leads to decrease in fabrication costs.

Advantages of organic solar cells [51];

- Safety
- Remotable
- Can be applied on the flexible substrates
- Relatively cheap in production and purification
- Can be shaped
- High absorption coefficient : low thickness of film as nanometer can be enough
- Potential for future growth

Disadvantages of organic solar cells are as follows [52];

- Requirement of economic energy storage system
- Expensive installation expenses
- Requirement of more research
- Limited lifetime

1.9.1. Donor-Acceptor Approach

Band gap engineering is crucial in order to manage band gap of materials since band gap affects optical and optoelectronic properties of polymers directly. In order to reach desired band gap, several parameters can be changed.

Conjugated polymers can have two forms in their ground state which are quinoid and aromatic. Quinoid character is important for charge transport and charge separation.

Quinoidal characteristic of polymer backbone decreases the band gap since quinoid character increases planarity and thus π electron delocalization gets easier [53].

Suitable conjugation size also can enhance π delocalization. Moreover, more stable polymers (thermally and chemically); high charge carrier mobility can be obtained by arranging conjugation size [54]. Excess conjugation length may decrease solubility and processability of polymers [53].

Side chains affect the intermolecular interaction between polymer chains and polymer fullerene interaction. Solubility of polymers can increase with side chains due to decreasing π - π interaction but excess decline of π - π interaction can lead to more steric hindrance. Thus, low charge transport can cause bad solar cell characteristics [53]. Moreover, substituents such as fluorine, cyano group and heteroatoms (i.e. Si,Se) can be added to the polymer backbone and it can affect the electronic properties of polymer.

The most important parameter is donor-acceptor approach for tuning of band gap. According to this approach, low band gap of polymers can be configured by using different type of donor (electron rich) and acceptor (electron deficient) groups. It is note taking to state that, although the aim of this approach is to form low band gap polymers, it can be adapted to form polymers with low, medium and large band gap. For OSC, high HOMO of donor match with low LUMO of acceptor and new low band gap energy is formed [55]. Schematic view of donor- acceptor approach is depicted in Figure 13.

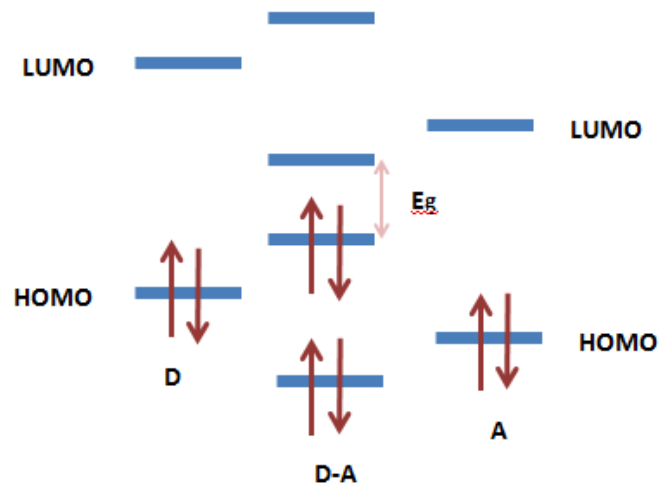


Figure 13. Schematic view of donor-acceptor approach

1.9.2. Basic Structure of OSC

Like OLED devices, OSC structure consists of metal as cathode, PEDOT:PSS as HTL and ITO as anode. The OSC device configuration is demonstrated in Figure 14. The structural difference derived from the blend active layer between OLED and OSC. For OLED, polymer is used as active layer. On the other hand, polymer is blended with fullerene derivatives to balance charge transfer for OSC. Except active material, the residue layers are the same as OLED's structure and detailed information was given at section 1.8.1.

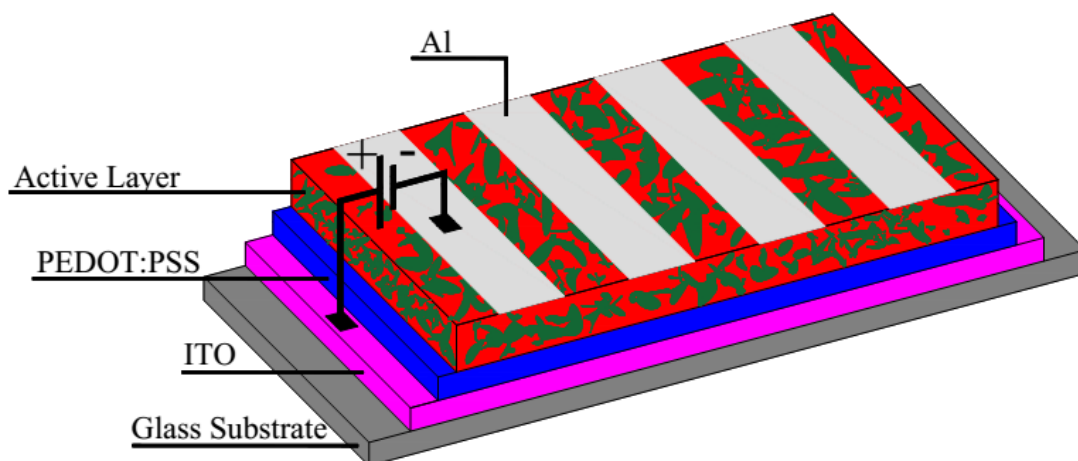


Figure 14. Demonstration of OSC device configuration

Generally, organic semiconductor materials are blended with a second material (e.g. fullerene derivatives) since it increases the efficiency of OSC devices [56]. Bicontinuous and interpenetrating donor-acceptor network is required for effective charge separation. Morphology is also important since little changes in morphology can cause traps for charges. Hence, recombination can be occurring [52].

Mobility of holes is higher than electrons. So, electron acceptors are preferred for D/A blend. With this aim, buckminsterfullerene (C_{60}) is used since it has excellent electron acceptor ability. In some cases, [6,6]-phenyl C61 butyric acid methyl ester ($PC_{61}BM$) and [6,6]-phenyl C71 butyric acid methyl ester ($PC_{71}BM$) can be better alternative since C_{60} is not soluble in common solvents [47].

1.9.3. Working Principle of OSC

Working principle of OSC is different than OLED. Basically, OSC produces energy by using sun light. On the other hand, OLED consumes energy in order to produce light. For OSC, light is absorbed and it leads to generation of excitons. Then, generated excitons diffuse near the D/A interface and lastly dissociated excitons are collected. It is depicted in Figure 15.

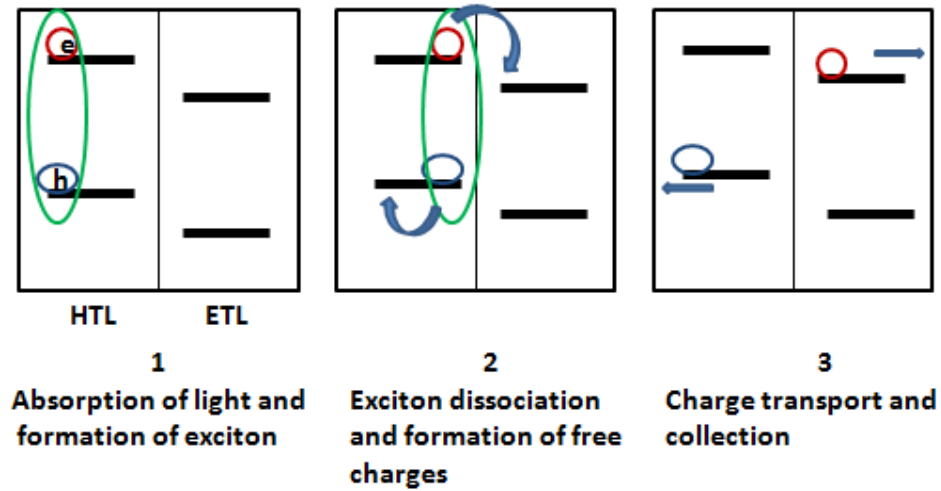


Figure 15. Working principle of OSC

There are 4 main steps [57].

1. Absorption of light and generation of exciton
2. Diffusion of excitons near the D/A interface
3. Dissociation of excitons
4. Collection of excitons

1.9.4. OSC Characterization

Characterization of OSC device can be identified by interpreting the graph of the current density-voltage (J - V) experimentally. J - V curve is defined under two conditions; Dark and illumination. If there is almost no current or potential, J - V curve run through the origin under dark conditions. On the other hand, power can be produced under illumination thus both current and voltage can be observed.

$$\eta = \text{PCE} = \frac{P_{\text{out}}}{P_{\text{in}}}$$

$$P_{\text{out}} = V_{\text{max}} \times J_{\text{max}}$$

$$\text{IPCE} = 1240 \frac{J_{\text{sc}}}{\lambda P_{\text{in}}}$$

$$P_{\text{out}} = V_{\text{oc}} \times J_{\text{sc}} \times FF \quad (5)$$

The ratio between generated maximum power of device (P_{out}) and incident power of solar spectrum (P_{in}) gives power conversion efficiency (η or EQE). EQE is also

interpreted as incident photon to current efficiency (IPCE) which is ratio between the incident photon to collected electron at specific wavelength (λ) [58]. The incident power is determined by using air-mass (AM) terminology. Generally, AM 1.5 G (air mass 1.5 global) is used as a standard for solar cell applications. Air mass defines the amount of incident light from sun through the surface of earth. According to AM 1.5 G standard, the angle between arrival sunlight and the earth's surface is accepted as 48° . Moreover intensity is taken 100 mW/cm^2 for OSC measurements [59]. Used terminologies are indicated in Figure 16 by using current-voltage curve under dark and illumination and equations are given in equation 5.

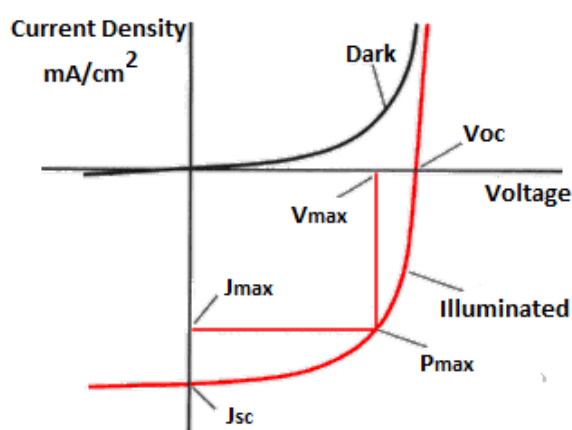


Figure 16. Current-voltage curve under dark and illumination

Open circuit voltage (V_{oc}) indicates the maximum voltage with no current flow. According to Brabec's study, V_{oc} is related to the LUMO energy level of acceptor. Moreover, according to Scharber's study, V_{oc} is also related to the HOMO level of the donor [59]. Thus, an equation was developed in order to calculate V_{oc} , and q shows elementary charge that is depicted in equation 6. Efficient charge transfer is calculated as 0.3 eV between LUMO levels of donor and acceptor and thus 0.3 eV is accepted as empirical factor [60].

$$V_{oc} = \frac{1}{q} [E(\text{HOMO})_{\text{donor}} - E(\text{LUMO})_{\text{acceptor}}] - 0.3 \quad (6)$$

Short circuit current (J_{sc}) defines the maximum current flow with no external voltage. Number of charge carriers and their mobility, band gap range and absorption coefficient affects the J_{sc} [59].

Fill factor (FF) is the percent ratio between the actual maximum obtainable power ($V_{max} \times J_{max}$) and theoretical power ($J_{sc} \times V_{oc}$) that is depicted in equation 7. Morphology, thickness, interfaces between electrodes and donor-acceptor, series resistance and shunt resistance affects the fill factor. Ideally, FF should equal to one theoretically.

$$FF = \frac{V_{max} \times J_{max}}{V_{oc} \times J_{sc}} \quad (7)$$

1.10. Benzotriazole Based Conjugated Polymers

The structure of benzotriazole (BTz) includes imide bond and it is accepted as medium acceptor unit because of its electron deficient characteristic. The reason of electron deficient nature is high lying LUMO energy level and it can lead to the increase of V_{oc} . It is also known as a benzoazole derivative due to nitrogen atom and it makes BTz basic and electron rich. Alkyl chain addition to the BTz is easy and this addition increases the solubility of the material. Easy modification of alkyl chain makes BTz preferable than quinoxaline and benzothiadiazole derivatives and high conversion efficiency can be obtained by using BTz derivatives [61]. Recently, 7% power conversion efficiency was recorded for OSC applications [62]. Structure of BTz with alkyl chain makes the material more planar due to prevention of steric hindrance. As a result, hole mobility increases thanks to close packing structure. Generally, benzotriazole derivatives are used for electrochromic applications since they indicate multichromism property [63].

Selenophene was used as π bridge electron donor cyclic groups. According to D-A approach, π bridge electron donor cyclic groups such as thiophene and selenophene were chosen in order to change electronic and optical properties of polymers. Selenophene has high quinoid property so it causes the low bond length alternation.

Thus, low band gap polymers can be obtained using selenophene. Moreover, selenophene has high intermolecular interaction because of its polarizable characteristic. Thereby, charge carrier transport ability can increase by using selenophene.

In literature orange emitting conjugated polymers can be used in order to design white OLEDs since combination of two colors (e.g. orange and blue) in a proper ratio can give exact white light [64]. By using benzotriazole based orange emissive layer with blendind blue donor, almost pure white light generation ($x=0.31$, $y=0.32$) can be obtained [65].

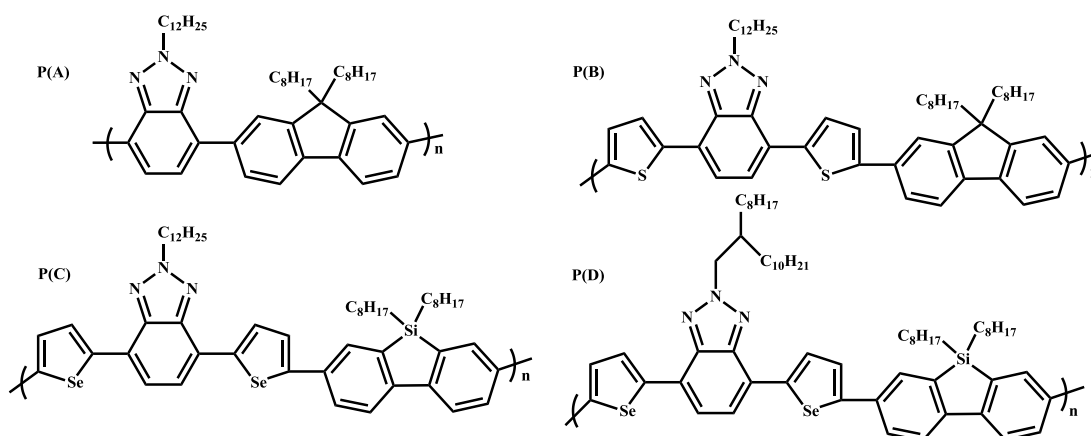


Figure 17. Some Literature Examples

For OSCs, small structural modifications make polymer quite different properties. With this purpose, donor acceptor approach has been used. For example, in 2010, benzotriazole unit was coupled with fluorene unit by Suzuki condensation reaction. At the same study, the thiophene unit was attached to the mentioned polymer and their electronic and optical properties were investigated. The results of this study proved that polymers have suitable band gaps and high absorption in visible region so they are good candidates for optoelectronic studies [66]. Their PCE is 0.07% for P(A) and 0.56% for P(B) [67]. By using selenophene as the bridge, the properties of polymers were improved and better results were obtained. From the literature, P(C)

and P(D) include similar acceptor units with **P1** and **P2** and silafluorene was used as donor unit. Both polymers have suitable band gap for an electrochromic application and their efficiencies are 1.55% for P(C) and 1.26% for P(D) [68]. According to donor acceptor approach, small molecular differences can make the polymers different electronic characteristics. Since P(C) and P(D) have moderately high efficiencies; benzotriazole with selenophene bridge can be good candidate to reach higher efficiencies by using different type of donor unit. The structure of the mentioned polymers in the literature is depicted in Figure 17 and their results are summarized in Table 2.

Table 2. The basic results of the studied polymers in literature [67,68].

	HOMO (eV)	LUMO (eV)	Eg(eV)	Optical contrast	Switching time (s)	Voc (V)	η (%)
P(A)	-5.94	-2.97	2.97	22% (1500 nm)	3.5	0.60	0.07
P(B)	-5.71	-3.15	2.56	39% (2000 nm)	3.3	0.60	0.56
P(C)	-5.31	-3.27	2.04	12% (1200 nm)	0.6	0.71	1.55
P(D)	-5.18	-3.12	2.06	23% (1200 nm)	1.0	0.63	1.26

In this study, dibenzene bridged donor units (fluorene and carbazole) were used. Dibenzene bridged donor units are known as weak donor units because of electron deficient characteristic of benzene. Integration of carbon, nitrogen or silicon to the polymer leads to moderately high band gap and narrow light absorption [69]. Although these properties can be trouble for OSC applications, they can suitable for

OLED applications. Fluorenes has rigid and planar structure. Polymers with fluorene generally have high band gap and low HOMO energy levels. Moreover, they are very stable to degradation against photon and heat; hence it can be a suitable candidate for device operation. The reason for the use of fluorene is that it indicates high fluorescence quantum yield, perfect hole transporting ability and excellent film forming features. Carbazole is very similar structure to fluorene and its central includes fused pyrrole with electron donating nitrogen atom. Thus, carbazole has tricyclic structure and it means that carbazole is a fully aromatic and electron rich compound. Like fluorene, carbazole also has stable thermally and photochemically and lastly high charge mobility. Chemical structures of donor and acceptor groups are shown in Figure 18.

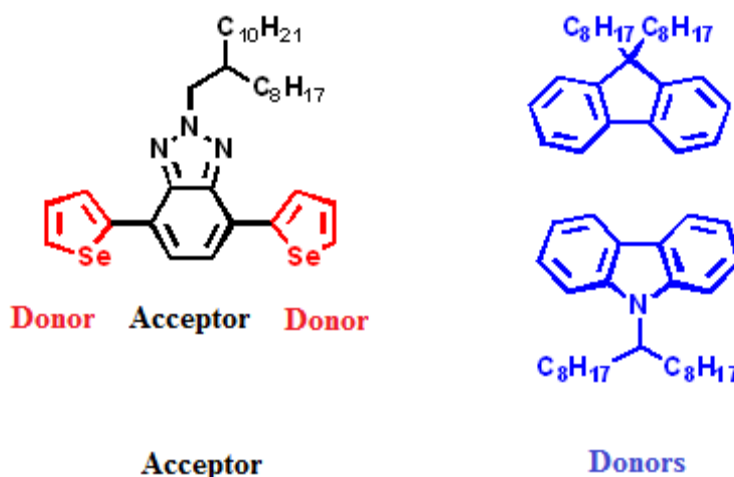


Figure 18. Chemical structures of donor and acceptor groups

1.11. Aim of Thesis

The purpose of the study is to synthesize polymers with broad light absorption and high fluorescent ability for both OSC and OLED applications. Donor- acceptor type new polymers were synthesized by anchoring different donor groups on the polymer backbone in order to provide high conversion efficiencies. These polymers were synthesized chemically and their electrochemical and device characterizations were investigated. Benzotriazole was used as an acceptor unit and it was coupled with

selenophene as a π bridge donor segment. The reason for the use of benzotriazole is its excellent electrochromic properties. Benzotriazole based polymers generally reveal multichromism which is important for electrochromic device applications [70]. Fluorene and carbazole were selected as the electron donating groups due to their excellent film forming properties, good hole transport ability and high thermal stability. Solubility of synthesized polymers was provided by using branched alkyl chain and their structure is depicted in Figure 19.

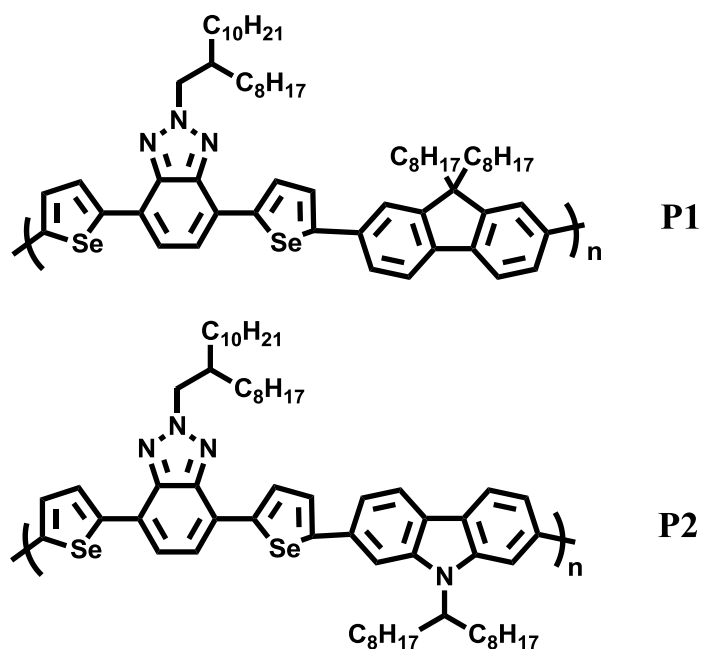


Figure 19. The molecular structures of synthesized polymers in this study

CHAPTER 2

EXPERIMENTAL

2.1. Materials and Equipments

All chemicals and solvents were supplied by Sigma Aldrich Chemical Co. Ltd. PC₇₁BM was obtained from Solenne. Tetrahydrofuran (THF) and toluene were dried by using metallic sodium and benzophenone. They were prepared before reactions and no dated solvents were used. All reactions were studied under argon atmosphere if not specifically defined otherwise.

Merck Silica Gel 60 was utilized for purification of synthesized materials. Structures of synthesized materials were verified by nuclear magnetic resonance (NMR) on a Bruker Spectrospin Avance DPX-400 Spectrometer by taking internal reference as trimethylsilane (TMS) in deuterated chloroform (CDCl₃). Gel permeation chromatography (GPC) was used to identify the average molecular weights of the polymers by taking polystyrene as the reference in chloroform (CHCl₃). Electrochemical studies were carried out by using Voltalab 50 potentiostat. Varian Cary 5000 UV-Vis spectrometer and Minolta CS-100 spectrometer were used for spectroelectrochemical and colorimetry application, respectively. OLED and OSC applications were performed in glove box system (MBraun) (both O₂ and H₂O < 0.1 ppm). INFICON SQC-310 Thin Film Deposition Controller was used to evaporation of cathode and LiF layers. While 1.5G illumination was used (100mV/cm²) for OSC characterization, D55 illuminant was applied for OLED applications. Graphs of current versus voltage and luminance versus voltage were recorded by using Keithley 2400 Source and Maya2000 PRO Spectrophotometer, respectively.

2.2. Synthetic Procedure

4,7-Dibromo-2-(2-octyldodecyl)-2H-benzo[d][1,2,3]triazole and tributyl(selenophen-2-yl)stannane were synthesized according to previously reported methods [71,72,73]. 2-(2-octyldodecyl)-4,7-di(selenophen-2-yl)-2H-benzo[d][1,2,3]triazole was brominated with NBS previously published procedures [68].

2.2.1. Synthesis of 9-(bromomethyl) nonadecane

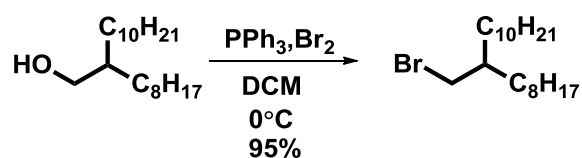


Figure 20. Synthesis of 9-(bromomethyl) nonadecane

2-Octyl-1-dodecanol (4.00 g, 13.4 mmol) and 15.0 mL DCM were stirred at 0 °C. After the addition of triphenylphosphine (PPh₃) (3.69 g, 14.1 mmol) at one portion, bromine (Br₂) (2.25 g, 14.1 mmol) in 5.00 mL DCM was added drop wise. The reaction was stirred for 5 hr at room temperature. Then, saturated NaHSO₃ solution was slowly added to the reaction medium in order to remove excess Br₂. Water was added and the mixture was extracted with DCM (3x). Then combined organic layers were washed with brine. Organic phase was dried using MgSO₄. After the solvent evaporation, white powder was obtained. Column chromatography was applied for crude product on silica gel with hexane. Colorless oil was obtained (4.60 g, Yield: 95.0 %). ¹H NMR (400 MHz, CDCl₃) δ 3.38 (d, *J* = 4.7 Hz, 2H), 1.60 – 1.46 (m, 1H), 1.33 – 1.04 (m, 32H), 0.81 (t, *J* = 6.8 Hz, 6H). ¹³C NMR (101 MHz, CDCl₃) δ 39.69, 39.50, 32.57, 31.93, 29.80, 29.65, 29.60, 29.57, 29.36, 29.32, 26.57, 22.70, 14.12. ¹H and ¹³C NMR spectra of product is depicted in Figure 44 and Figure 45.

2.2.2. Synthesis of 4, 7-dibromobenzo[c][1, 2, 5] thiadiazole

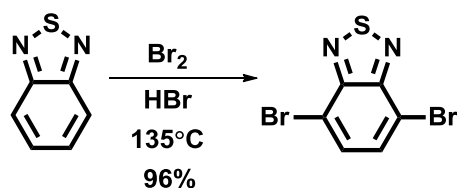


Figure 21. Synthesis of 4, 7-dibromobenzo[c][1,2,5] thiadiazole

Under ambient conditions 2,1,3-benzothiadiazole (5.00 g, 36.7 mmol) was dissolved in 45.0 mL HBr (47%). It was heated to 100°C and it refluxed for 1 hr. Then, bromine (Br_2) (17.3 g, 108.3 mmol) in 20.0 mL HBr (47%) was added slowly in dissolved 2,1,3-benzothiadiazole solution. It was heated under reflux for 12 hr at 135°C . TLC control (DCM) was used to probe the completion of reaction. After reaction was cooled to room temperature, concentrated NaHSO_3 was added slowly to the reaction medium. It was filtrated and washed with distilled water and cold diethyl ether, respectively. After the drying of residue, a yellow solid was obtained (10.4 g, Yield: 96.0%). ^1H NMR (400 MHz, CDCl_3) δ 7.73 (s, 2H). ^{13}C NMR (101 MHz, CDCl_3) δ 152.97, 132.36, 113.92. ^1H and ^{13}C NMR spectra of product is depicted in Figure 48 and Figure 49.

2.2.3. Synthesis of 3, 6-dibromobenzene-1, 2-diamine

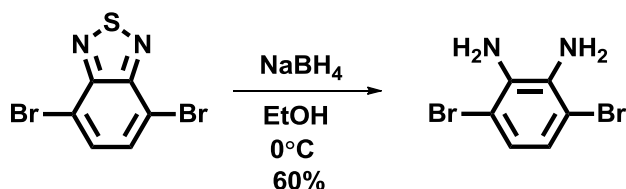


Figure 22. Synthesis of 3, 6-dibromobenzene-1, 2-diamine

4, 7-Dibromobenzo[c][1,2,5] thiadiazole (5.55 g, 18.9 mmol) was dissolved in 400 mL ethanol (EtOH) under ambient conditions. Before the NaBH_4 (10.1 g, 377 mmol) addition, the system was placed in an ice bath. When the temperature of system was

adjusted to the 0 °C, NaBH₄ was added slowly. After the addition was completed, the system was stirred for 12 hr at room temperature. Then, ethanol was evaporated and residual dark orange solid was dissolved in diethyl ether and washed with distilled water three times. Lastly, it was washed with brine. Organic phase was dried over MgSO₄ and the solvent was evaporated. Weight of dried residual light yellow solid was 3.00 g and used without further purification (3.00 g, Yield: 59.8 %).

2.2.4. Synthesis of 4, 7-dibromo-2H-benzo[d] [1, 2, 3] triazole

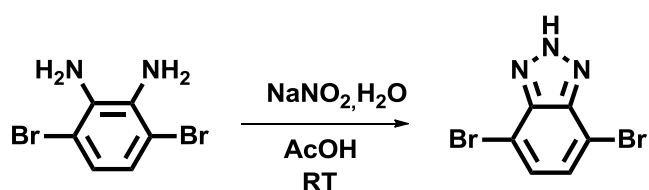


Figure 23. Synthesis of 4, 7-dibromo-2H-benzo[d] [1,2,3] triazole

3, 6-Dibromobenzene-1,2-diamine (3.00 g, 11.3 mmol) was dissolved in 30.0 mL acetic acid. At the same time, NaNO₂ (0.856 g, 12.41 mmol) was dissolved in 20.0 mL distilled water. Then, dissolved NaNO₂ added in dissolved 3,6-dibromobenzene-1,2 diamine quiet slowly. The mixture was stirred for 1 hr and precipitation was observed. Then, the precipitate was filtered and washed with distilled water. Lastly, the light orange powder solid was obtained. (3.12 g, Yield: 60.0%). ¹H NMR (400 MHz, CDCl₃) δ 7.44 (s, 2H), (Figure 50).

2.2.5. Synthesis of 4, 7- dibromo- 2- (2-octyldodecyl)-2H-benzo[d] [1, 2, 3] triazole

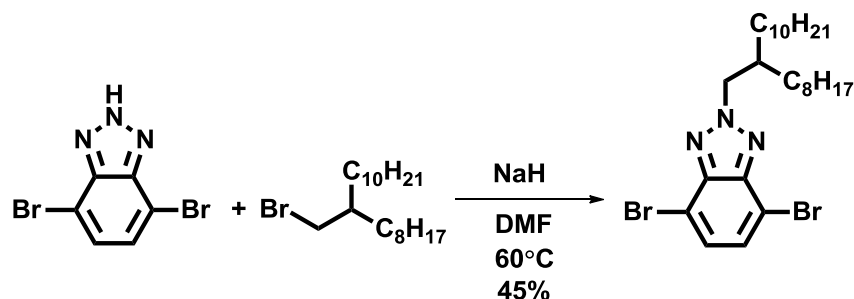


Figure 24. Synthesis of 4, 7- dibromo- 2- (2-octyldodecyl)-2H-benzo[d] [1,2,3] triazole

4, 7-Dibromo-2H-benzo[d] [1,2,3] triazole (2.59 g, 9.35 mmol) was dissolved 10.0 mL anhydrous DMF at 0°C under argon. After DMF addition, bubbling was applied for 15 min. Then, NaH (0.263 g, 10.9 mmol) was added at one portion. When NaH was dissolved completely, the system was heated to 60 °C. After the temperature was adjusted to 60 °C, 9-(bromomethyl) nonadecane (3.94 g, 10.9 mmol) was added into reaction medium and stirred for 12 hr. Then, DMF was evaporated and residue was dissolved in CHCl₃ and washed with distilled water at three times. Solvent was evaporated and column chromatography on silica gel was adjusted for purification of material (4:1 Hexane: CHCl₃). Tint yellow oil was obtained (2.35 g, Yield: 45.0 %). ¹H NMR (400 MHz, CDCl₃) δ 7.43 (s, 2H), 4.68 (m, 2H), 2.35 (m, 1H), 1.40 – 1.16 (m, 32H), 0.87 (m, 6H); (Figure 51). ¹³C NMR (101 MHz, CDCl₃) δ 143.64, 129.40, 110.00, 61.12, 39.02, 31.88, 31.18, 29.87, 26.03, 22.66, 14.10; (Figure 52).

2.2.6. Synthesis of tributyl (selenophen-2-yl) stannane

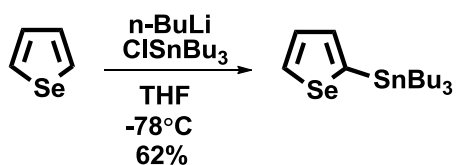


Figure 25. Synthesis of tributyl (selenophen-2-yl) stannane

Selenophene (5.00 g, 38.2 mmol) was deaerated with argon for 15 min to remove O₂ from reaction medium. Dry THF was added and the system was adjusted to - 78°C and n-buthyl lithium (n-BuLi) (2.5 M in hexane, 16.8 mL, 41.9 mmol) was added drop wise into the reaction medium and stirred for 1 hr. Reaction color turned to light pink from colorless. Then, stannyltributyltin chloride (ClSnBu₃) (11.4 mL, 41.9 mmol) was added. The color of the reaction was dark orange, and then it turned to milky brown. Then, the reaction was stirred under argon atmosphere for 12 hr at room temperature. Later on, THF was evaporated and residue was dissolved in CHCl₃. It was washed with distilled water and organic phase was dried over MgSO₄. After CHCl₃ was evaporated, neutral alumina column chromatography was performed with hexane. Colorless oil was obtained (10.0 g, Yield: 62.0%). ¹H NMR (400 MHz, CDCl₃) δ 8.25 (dd, *J* = 10.8, 4.6 Hz, 1H), 7.45 – 7.36 (m, 2H), 1.57 – 1.45 (m, 6H), 1.31 – 1.22 (m, 6H), 1.06 – 0.98 (m, 6H), 0.82 (m, 9H); (Figure 46). ¹³C NMR (101 MHz, CDCl₃) δ 143.58, 137.99, 135.33, 130.70, 29.33, 27.63, 27.34, 11.23; (Figure 47).

2.2.7. Synthesis of 2-(2-octyldodecyl)-4, 7-di (selenophen-2-yl)-2H-benzo [d] [1, 2, 3] triazole

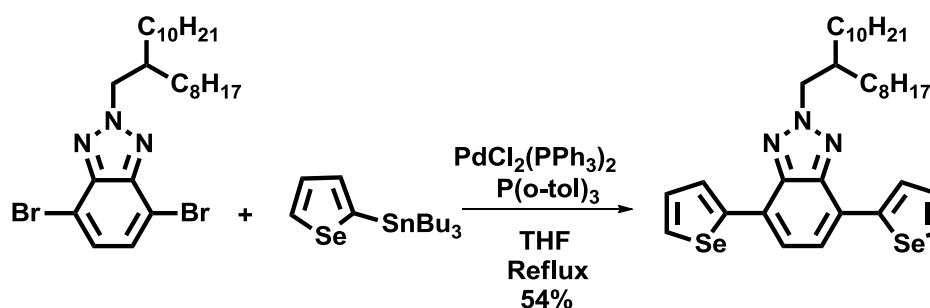


Figure 26. Synthesis of 2-(2-octyldodecyl)-4, 7-di (selenophen-2-yl)-2H-benzo [d] [1,2 3] triazole

4,7-Dibromo-2-(2-octyldodecyl)-2H-benzo[d][1,2,3] triazole(1.15g, 2.06 mmol) and tributyl(selenophen-2-yl)stannane (1.74 g, 4.13 mmol) were added in a two neck round bottom flask and stirred for 15 min under argon. Then, 20.0 mL THF were

added in the flask and bubbling was applied using argon for 1 hr. After the addition of bis(triphenylphosphine)palladium(II) dichloride (0.094 g, 0.825 mmol) and tri-tolylphosphine (0.251 g, 40 mol %) in reaction medium it was refluxed for 20 hr. Then, solvent was evaporated and residue was purified by column chromatography on silica gel with hexane and chloroform (4:1) system. A solid was obtained as a yellow product (0.90 g, Yield: 54.0 %), (Figure 26). ^1H NMR (400 MHz, CDCl_3) δ 8.11 (d, $J = 3.2$ Hz, 2H), 8.00 (d, $J = 5.6$ Hz, 2H), 7.52 (s, 2H), 7.33 (dd, $J = 5.6, 3.2$ Hz, 2H), 4.66 (d, $J = 6.4$ Hz, 2H), 2.24-2.18 (m, 1H), 1.35 – 1.15 (m, 32H), 0.83 – 0.77 (m, 6H), (Figure 53). ^{13}C NMR (101 MHz, CDCl_3) δ 141.58, 133.56, 127.06, 121.63, 117.74, 106.50, 67.97, 29.68, 29.35, 28.27, 26.76, 22.68, 17.29, 14.11, 13.57, (Figure 54).

2.2.8. Synthesis of 4, 7-bis (5-bromoselenophen-2-yl)-2-(2-octyldodecyl)-2H-benzo[d][1,2,3]triazole

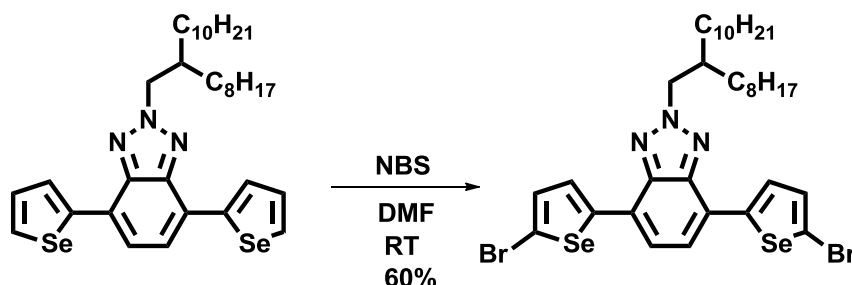


Figure 27. Synthesis of 4, 7-bis (5-bromoselenophen-2-yl)-2-(2-octyldodecyl)-2H-benzo[d][1,2,3] triazole (**M1**)

2-(2-Octyldodecyl)-4,7-di(selenophen-2-yl)-2H-benzo[d][1,2,3] triazole (250 mg, 0.380 mmol) was dissolved in 10.0 mL dry DMF under argon. After complete dissolution, N-bromosuccinimide (NBS) (176 mg, 0.989 mmol) was slowly added under dark medium. The reaction medium was stirred for 12 hr. Purification was applied by using column chromatography by silica gel with hexane and ethyl acetate (15:1) and a dark yellow solid was obtained (186 mg, Yield: 60.0 %), (Figure 27). ^1H NMR (400 MHz, CDCl_3) δ (ppm) 7.70 (d, $J = 4.2$ Hz, 2H), 7.46 (s, 2H), 7.25 (d, $J = 4.2$ Hz, 2H), 4.65 (d, $J = 6.3$ Hz, 2H), 2.23 – 2.13 (m, 2H), 1.29 – 1.14 (m, 32H),

0.82 – 0.78 (m, 6H), (Figure 55). ^{13}C NMR (101 MHz, CDCl_3) δ 178.53 , 134.70 , 132.58 , 130.62 , 128.46, 127.21 , 126.88 , 123.04 , 32.41 , 31.55 , 29.90, 29.56 , 29.34 , 26.55 , 22.68 , 14.11, (Figure 56).

2.2.9. Synthesis of 4-(5-(7-methyl-9,9-dioctyl-9H-fluoren-2-yl)-7-(5-methylselenophen-2-yl)-2-(2-octyldodecyl)-2H-benzo[d][1,2,3]triazole (P1)

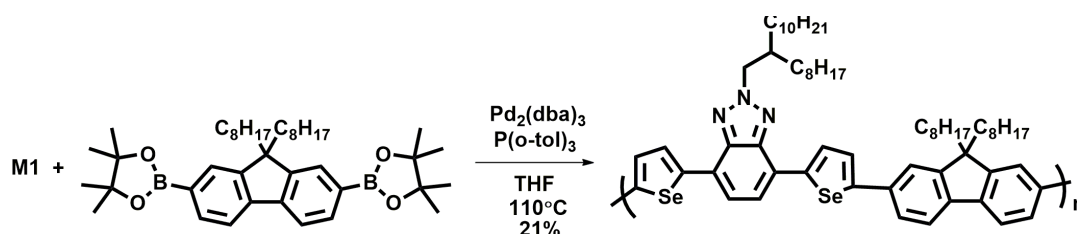


Figure 28. Synthesis of 4-(5-(7-methyl-9,9-dioctyl-9H-fluoren-2-yl)-7-(5-methylselenophen-2-yl)-2-(2-octyldodecyl)-2H-benzo[d][1,2,3] triazole (P1)

K_2CO_3 (2 M, 2.5 mL) solution was added in 100 mL two neck round bottom flask and it was stirred for 30 min under argon. Then, 7.50 mL dry THF and 4,7-bis(5-bromoselenophen-2-yl)-2-(2-octyldodecyl)-2H-benzo[d][1,2,3] triazole (200 mg, 0.249 mmol) and 2,2'-(9,9-dioctyl-9H-fluorene-2,7-diyl)bis(4,4,5,5-tetramethyl-1,3,2-dioxaboralane) (139 mg, 0.249 mmol) were added to the flask. After the system was purged with argon for additional 30 minutes, addition of tris(dibenzylideneacetone)dipalladium(0) ($\text{Pd}_2(\text{dba})_3$) (18 mg, 5.0 mol%), tris(*o*-tolyl)phosphine (48.3 mg, 40 mol%) and catalytic amount aliquat 336 (phase transfer agent) was completed into the flask. At the same time, the temperature was adjusted to 110°C . The reaction was refluxed at 110°C for 40 hr. After that, bromobenzene (0.187 mg) and 3.00 mg additional $\text{Pd}_2(\text{dba})_3$ were added. The mixture was stirred for another 4 hr. After the addition of phenyl boronic acid (0.290 mg, 0.239 mmol), the reaction was stirred for 12 hr. Then, the reaction was cooled to the room temperature and toluene was evaporated under reduced pressure. The residue was precipitated in methanol, and filtered. The residue was purified by using Soxhlet apparatus with acetone, hexane, chloroform and chlorobenzene, respectively until the solvent in

Soxhlett becomes colorless. Lastly, collected chloroform was evaporated under reduced pressure and precipitation of the residue in cold methanol was filtered. Then pure polymer was dried with vacuum drying (55.0 mg, Yield: 21.0 %). GPC: number average molecular weight (Mn): 17900, molecular average molecular weight (Mw): 36800, polydispersity index (PDI): 2.05 ¹H NMR (400 MHz, CDCl₃), δ (ppm): 8.1-8.3 (2H, BTz), 7.3-7.8 (10H, selenophene-fluorene), 4.75 (2H, N-CH₂, BTz), 2.29 (1H, -CH), 1.4-0.9 (-CH₂, -CH₃), (Figure 57).

2.2.10. Synthesis of 9-(heptadecan-9-yl)-2-methyl-7-(5-(7-(5-methyl selenophen-2-yl)-2-(2-octyldodecyl)-2H-benzo[d][1,2,3]triazol-4-yl) selenophen – 2 -yl)-9H-carbazole (P2)

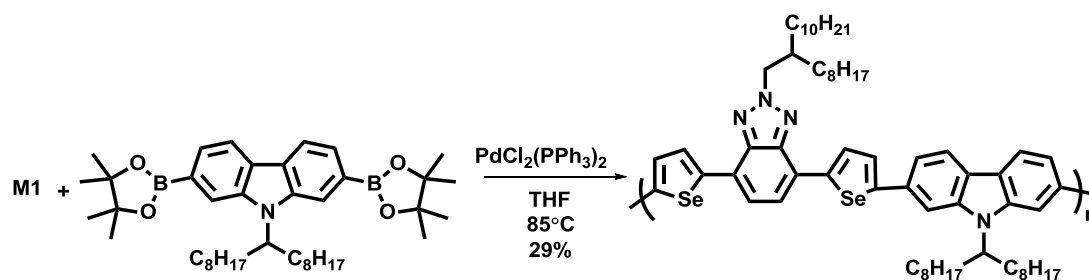


Figure 29. Synthesis of 9-(heptadecan-9-yl)-2-methyl-7-(5-(7-(5-methyl selenophen-2-yl)-2-(2-octyldodecyl)-2H-benzo[d][1,2,3]triazol-4-yl) selenophen – 2 -yl)-9H-carbazole (P2)

K₂CO₃(2 M, 5.0 mL) solution was added in 100 mL two neck round bottom flask and it was stirred for 30 min under argon. Then, 10.0 mL dry THF and 4, 7-bis (5-bromoselenophen-2-yl)-2-(2-octyldodecyl)-2H-benzo [d][1,2,3] triazole (295 mg, 0.362 mmol) and (2-(9-(heptadecan-9-yl)-7-(4,4,5,5-tetramethyl-1,3,2-dioxaborolan-2-yl)-9H-carbazol-2-yl)-4,5,5-trimethyl-1,3,2-dioxaborolan-4-yl)methylum (241 mg, 0.362 mmol) were added to the flask under argon atmosphere. After the system was purged with argon for additional 30 minutes, addition of bis (triphenylphosphine) palladium (II) dichloride (PdCl₂(PPh₃)₂) (12.7 mg., 5.0 mol%) and tetra-n-hexyl ammonium iodide (8.71 mg, 5.0 mol%) were completed. At the same time, the temperature was adjusted to 85 °C. The reaction was refluxed at 85 °C

for 20 hr. After that, bromobenzene (30.0 mg, 0.191 mmol) and 3.00 mg additional (Pd(Cl₂) (PPh₃)₂) were added. The mixture was stirred extra for 4 hr. After the addition of phenyl boronic acid (60.0 mg, 0.490 mmol), the reaction was stirred for 12 hr. Then, the reaction was cooled to room temperature and THF was evaporated under reduced pressure. The residue was precipitated in methanol, and filtration was applied. The residue was purified by using Soxhlet apparatus with acetone, hexane, chloroform and chlorobenzene respectively, until the solvent in Soxhlet becomes colorless. Lastly, collected chloroform was evaporated under reduced pressure and precipitation of the residue in cold methanol was filtered. Then pure polymer was dried with vacuum drying (110 mg, Yield: 29.0 %). GPC: number average molecular weight (M_n): 10816, molecular average molecular weight (M_w): 71600, polydispersity index (PDI): 6.62. ¹H NMR (400 MHz, CDCl₃), δ (ppm): 8.21(2H, BTz), 8.1-8.0 (2H, carbazole), 7.8-7.3(selenophene, carbazole), 4.68 (N-CH₂, BTz), 2.49-1.81 (-CH₂), 1.69-0.43 (-CH₃), (Figure 58).

2.3. Electrochemical Studies

During redox reactions, materials can gain different colors. If the color change is significantly distinct, the species can be called as electrochromic materials [74].

HOMO and LUMO energy levels can be estimated experimentally for organic thin films by using cyclic voltammetry (CV). CV is a three electrode system with an ITO as the working electrode (WE), platinum as the counter electrode (CE) and Ag wire as the reference electrode (RE). The polarity of the given potential determines whether the films are to be oxidized or reduced. So, the value of applied potential must be enough to begin charge transfer by increasing or decreasing the Fermi energy level of the WE. Before measurements, the electrolyte solution was bubbled with argon in order to get rid of dissolved oxygen. Redox properties of polymer coated thin film are investigated via single scan cyclic voltammogram. HOMO level of the polymer can be determined by onset oxidation potential and similarly, LUMO level of the polymer can be determined by LUMO level of the polymer. Energy

difference between HOMO and LUMO energy levels defines the electronic band gap of polymer (equation 8) [75].

$$HOMO = -(4.75 + E_{ox}(onset))$$

$$LUMO = -(4.75 + E_{red}(onset))$$

$$E_g = HOMO - LUMO \quad (8)$$

2.4. Spectroelectrochemical Studies

Spectroelectrochemical studies enlighten about the electrochromic properties of conjugated polymers. In this study, spray coated polymer films were oxidized step wise under applied potential. During this doping process, polarons and bipolarons (radical carriers) are formed. This process can be investigated in situ UV-Vis-NIR spectra as a function of external voltage. The π - π^* interband transitions of polymers is a distinctive property in their neutral states. The intensity of neutral band lessens and new bands are formed due to polarons with lower energy. If oxidation continues after formation of polaron, bipolarons also can exist. By taking a tangent line from the π - π^* interband transition, maximum absorption wavelength of polymer onsets (λ_{max}^{onset}) were determined and optical band gap of polymers were calculated (equation 9).

$$(E_g^{op}) = 1241 / \lambda_{onset} \quad (9)$$

2.5. Kinetic Studies

The kinetic studies were performed to observe the transmittance change with a time interval between maximum absorption wavelength of neutral and fully oxidized states of polymer films during potential sweeps. Thus, optical contrasts of polymer

films at their own maximum absorption wavelengths were determined by UV-Vis-NIR spectrophotometer. Moreover, switching times of polymer films were measured using chronoamperometry.

2.6. Gel Permeation Chromatography

Gel permeation chromatography (GPC) is important separation technique that based on size exclusion. In other words, molecular weight distributions such as number average molecular weight, weight average molecular weight can be identified on the basis of their size. GPC includes a column (solid stationary phase) with tiny, round, porous particles and the solvent (liquid mobile phase) passed through them. Small chains come later than the bigger ones since small chains can enter pores of the column. Polymers were dissolved in CHCl_3 (4.0 mg/mL) and their molecular weight distributions were determined.

2.7. OLED Studies

ITO coated glass substrates were purchased from Vision-Tek and used as the anode. Etching was carried out to eliminate short circuit of device. ITO coated glass sheets were cut (2.45 cm x 2.45 cm) and active area of ITO was protected. Protected ITO is immersed in 37 % concentrated hydrochloric acid (12 M), nitric acid and water, respectively for 3 minutes. Etched ITO substrates were cleaned with toluene, detergent (Hellmanex III) and water, acetone and 2-propanol in ultrasonic bath. In order to remove solvents, N_2 gas was purged. Lastly, oxygen plasma treatment was performed in order to remove organic contaminants. Therefore, the treatment helped to increase work function of ITO and made the surface hydrophilic.

PEDOT:PSS was used as HTL and it was filtered with 0.45 μm PVDF filter before coating process. By using G3 P-8 spin coater, it was coated with 5000 rpm for 45 seconds onto ITO substrates. Coated material was heated at 135°C for 15 minutes in order to remove solvent. Resulting thickness of PEDOT:PSS was 40 nm. Polymers were dissolved in CHCl_3 with 2 % weight concentration and it was filtered through 0.22 μm PTFE (teflon) membrane filter since this filter is chemically inert.

Polymers were coated with 2000 rpm for 45 seconds with a thickness of about 60 nm.

Lastly, both lithium fluoride (LiF, 0.6 nm) and aluminum (Al, 100 nm) were evaporated using evaporation chamber of Glove Box System (MBRAUN MB-200B). LiF was used as an auxiliary energy step between emissive layer and cathode. It also decreased the effective work function of aluminum. Emissive layer was protected from hot Al during thermal evaporation [56]. After the deposition of LiF, Al was evaporated as the cathode material. It protected the device from oxidation. As a result the device area of fabricated PLED was 0.06 cm². Constructed devices can be encapsulated in glass with epoxy resin in order to avoid O₂ and humidity.

PL properties of polymers were investigated via Perkin-Elmer LS 55 luminescence spectrometer by using the dilute polymer solutions with CHCl₃ and thin film samples. Maximum absorption wavelengths of polymers were selected as the excitation wavelengths for PL study. By using Spectrasuite (spectroscopy software) and Maya Pro 2000 spectrometer EL spectra, *J-V* curve were accomplished. Luminance of devices and CIE diagrams were carried out by using fiber optic in dark room.

2.8. OSC Studies

Etching and cleaning procedures of ITO were carried out as explained in section 2.7. **P2:PC**₇₁**BM** blends were prepared with different weight ratios and they were coated by using G3P-8 spin coater in glove box system (concentrations of O₂ and H₂O < 1 ppm). The structural order of constructed bulk heterojunction OSC devices were ITO/PEDOT:PSS/**P2:PC**₇₁**BM**/LiF/Al. The active area of OSC device was 0.06 cm². By using Keithley 2400 source meter with AM 1.5 G irradiation from a 1 kW Atlas Material Testing Solar Simulator, properties of *J-V* were determined. IPCE was measured by scanning between 300 nm and 1000 nm by using monochromic light.

CHAPTER 3

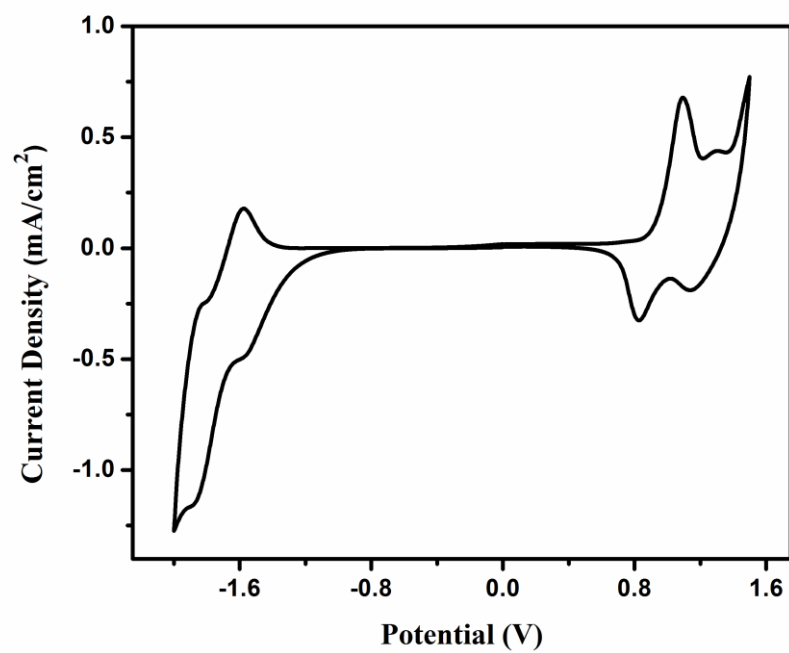
RESULTS AND DISCUSSIONS

3.1. Electrochemical Properties

After the polymers were dissolved in CHCl_3 solution (5 mg / mL), ITO was coated with polymer solution by spray coating technique. A three electrode system in 0.1 M TBAPF_6 in acetonitrile solution was used in order to investigate electrochemical properties of polymers as indicated in Figure 30. Then, HOMO and LUMO energy level of polymers were calculated by using oxidation and reduction onset potentials (E_{onset}). Both **P1** and **P2** indicated ambipolar (both p and n dopable) character. By using equation 8 that described in section 2.3, HOMO and LUMO energy levels were calculated.

For **P1**, potentials between -1.5 V and 2.0 V were scanned with 100 mV/s scan rate. There are two p doping processes at 1.09 V and 1.30 V. Due to the ambipolar character of **P1**, LUMO energy level was also calculated by using equation 8. For **P2**, potential was swept between -2.0 V and 1.4 V with 100 mV/sec scan rate and similar calculations were done.

a.



b.

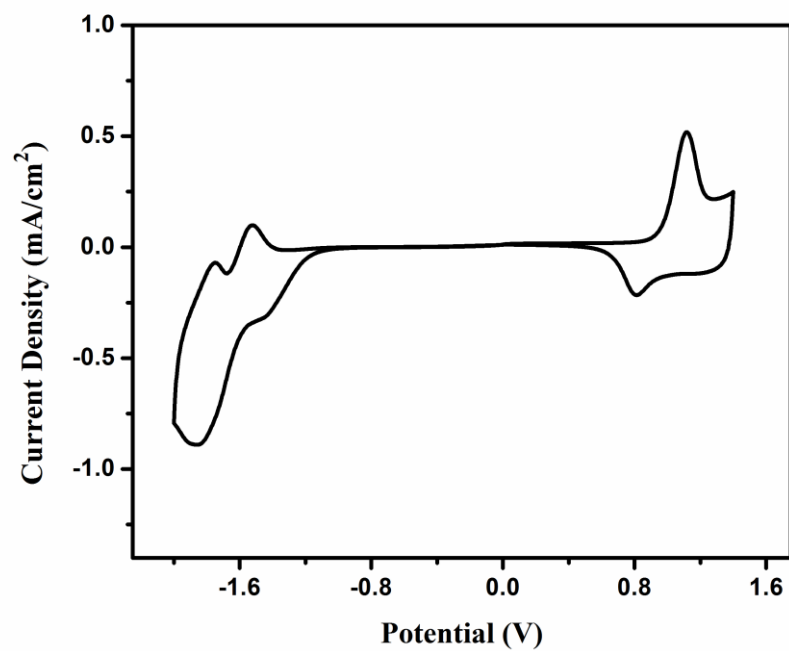


Figure 30. Single scan cyclic voltammograms of polymer films in 0.1 M TBAPF₆/ACN electrolyte solution (a) **P1** (b) **P2**

As a result, oxidation potentials of **P1** were determined at 1.09 V and 1.30 V with dedoping peaks at 0.83 V and 1.14 V. Likewise, reduction potentials was established at -1.87 V with a dedoping peak at -1.58 V. HOMO and LUMO energy levels were calculated as -5.66 V and -3.21 V respectively. Oxidation potentials of **P2** were found at 1.12 V with a dedoping peak at 0.81 V. Similarly, reduction potential was observed at -1.86 V with a dedoping peak at -1.52 V. HOMO and LUMO energy levels were calculated as -5.74 V and -3.34 V, respectively. **P1** indicated higher HOMO energy level than **P2** because **P1** had lower oxidation potential than **P2**. Although higher HOMO energy level causes to lower V_{oc} , it provides a lower band gap. All results were summarized in Table 3.

Table 3. Photophysical and electrochemical properties of polymers

	P1	P2
$E_{p-doping}$ (V)	1.09/1.30	1.12
$E_{p-dedoping}$ (V)	0.83/1.14	0.81
$E_{n-doping}$ (V)	-1.87	-1.86
$E_{n-dedoping}$ (V)	-1.58	-1.52
HOMO (eV)	-5.66	-5.74
LUMO (eV)	-3.21	-3.34
E_g^e (eV)	2.45	2.40

3.2.Optical Properties

The optical characteristics of **P1** and **P2** were studied in order to investigate the absorption range of polymers in their solution ($CHCl_3$) and in thin film form as indicated in Figure 31. Maximum wavelengths were 488/521 nm for **P1** and 486/522 nm for **P2** in their film form. In solution, maximum wavelengths were observed at 464 nm for **P1** and 483 nm for **P2**. All results were summarized in Table 4. The absorption spectra of thin film for polymers indicated red shift relative to the one recorded in solution. In solid state increased molecular orientation due to regular structure of thin film caused red shift with planarity effect in solid state [76]. The π - π

stacking was observed due to diminishing intermolecular distance and red shift was observed in the UV-vis absorption spectra [77,78]. Another reason of red shift might be that exist no pre-aggregation in solution. Although different types of donors were used, the polymers had similar optical properties.

Table 4. Optical properties of **P1** and **P2**

	Solution λ_{\max} (nm)	Thin film λ_{\max} (nm)
P1	464	488/521
P2	483	486/522

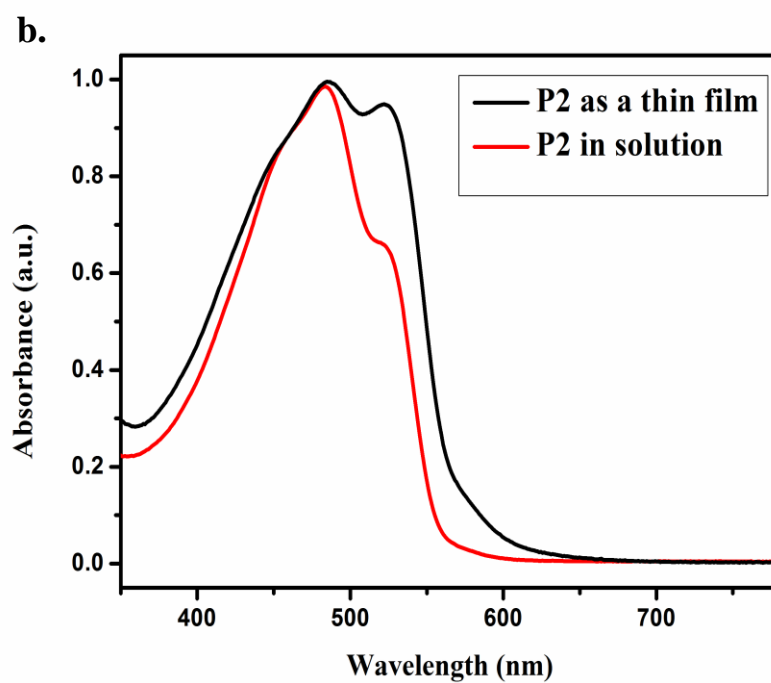
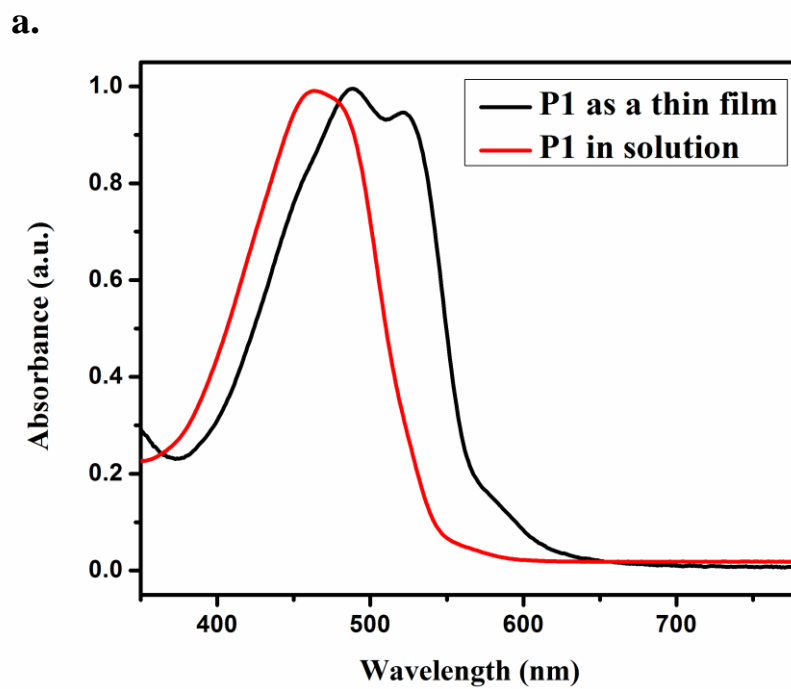


Figure 31. Normalized absorption spectra of (a) **P1** and (b) **P2** in chloroform and in the thin film

3.3. Scan Rate Studies

Anodic and cathodic current densities of spray coated thin films of polymers were investigated by applying different scan rates. Scan rate (v)-current density (i_p) graphs of polymers indicated that mass transfer of anions was not diffusion controlled as regards to Randles-Sevcik equation (equation 9) where i_p is current density (mA/cm^2), n is number of electrons, F is the diffusion coefficient (cm^2/s), v is potential sweep rate (mV/s), A is surface area of working electrode (cm^2), Γ is surface coverage of redox species (mol/cm^2), R is the gas constant, T is temperature in K [11,69,70,79].

$$i_p = n^2 F^2 v A \Gamma / 4RT \quad (9)$$

Scan rate graphs of **P1** and **P2** were depicted in Figure 32. The linear relationships between the current density-scan rate graphs proved that adherence of the polymer to the ITO surface were successfully achieved; anions and cations were located on the polymer chains. Thus, there was no diffusion where the electrochemical processes occurred reversibly.

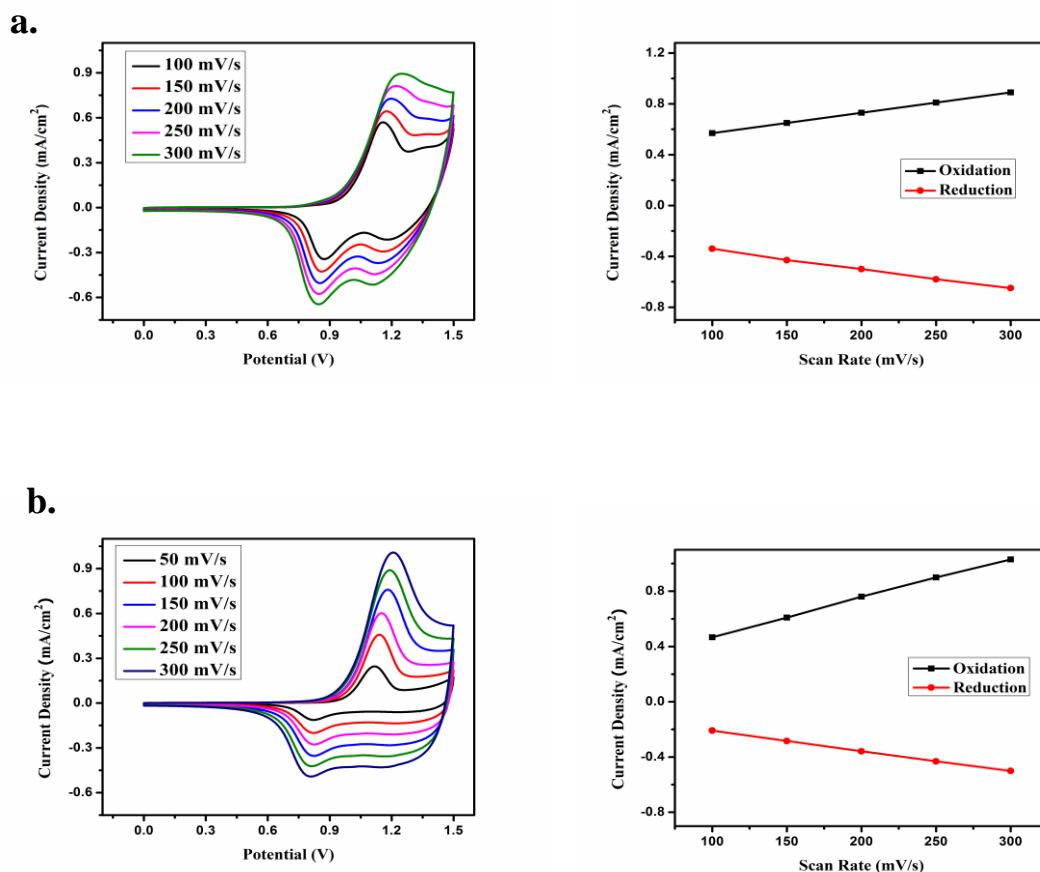


Figure 32. The scan rates studies in 0.1 M TBAPF₆ / ACN at scan rates of 100, 150, 200, 250 and 300mV/s for (a) **P1** and (b) **P2**

3.4. Spectroelectrochemical Properties of Polymers

The aim of the spectroelectrochemical studies was to explore the optical changes through doping-dedoping processes. Firstly, polymer solutions were prepared in chloroform (5 mg/mL) and they were coated on ITO glass via spray coating technique. They were placed in 0.1 M TBAPF₆/ACN electrolyte solution. Then, absorption spectra of polymers were investigated in UV-Vis-NIR regions under increasing external voltage. In Figure 33, the maximum absorption peak was observed at 522 nm with 594 nm onset wavelength for **P1** and 524 nm with 580 nm onset wavelength for **P2** in visible region. Then, optical band gaps (E_g^{op}) of polymers

were calculated as 2.09 eV for **P1** and 2.12 eV for **P2** by using equation 9 in section 2.4.

Maximum absorbance wavelengths were 720 nm and 710 nm in polaron region, 1500 nm and 1940 nm in bipolaron region for **P1** and **P2**, respectively. All results for **P1** and **P2** were very similar to each other since fluorene was structurally analogous to carbazole. The π - π^* transitions between the HOMO and LUMO levels of the polymers caused the first absorbance peak to be obtained in visible region. During oxidation, absorbance decreased in neutral state and the intensity of band increase both polaron and bipolaron regions. According to electrochemical studies, electrical band gaps were calculated as 2.45 eV and 2.40 eV for **P1** and **P2**, respectively. Optical band gap values were equal to 2.09 eV for **P1** and 2.12 eV for **P2**. Free charges were obtained during doping-dedoping process by cyclic voltammogram and electronic band gaps were determined via onset potentials of polymers. For optical band gap determination, light was absorbed and excitons formed. Then, onset of π - π^* transitions were used to calculate the optical band gap. As a result, while neutral state of polymers was used for optical band gap determination, doped-dedoped polymers were used for electronic band gap determination. Thus, optical band gaps of the polymers were comparatively lower than electronic band gaps.

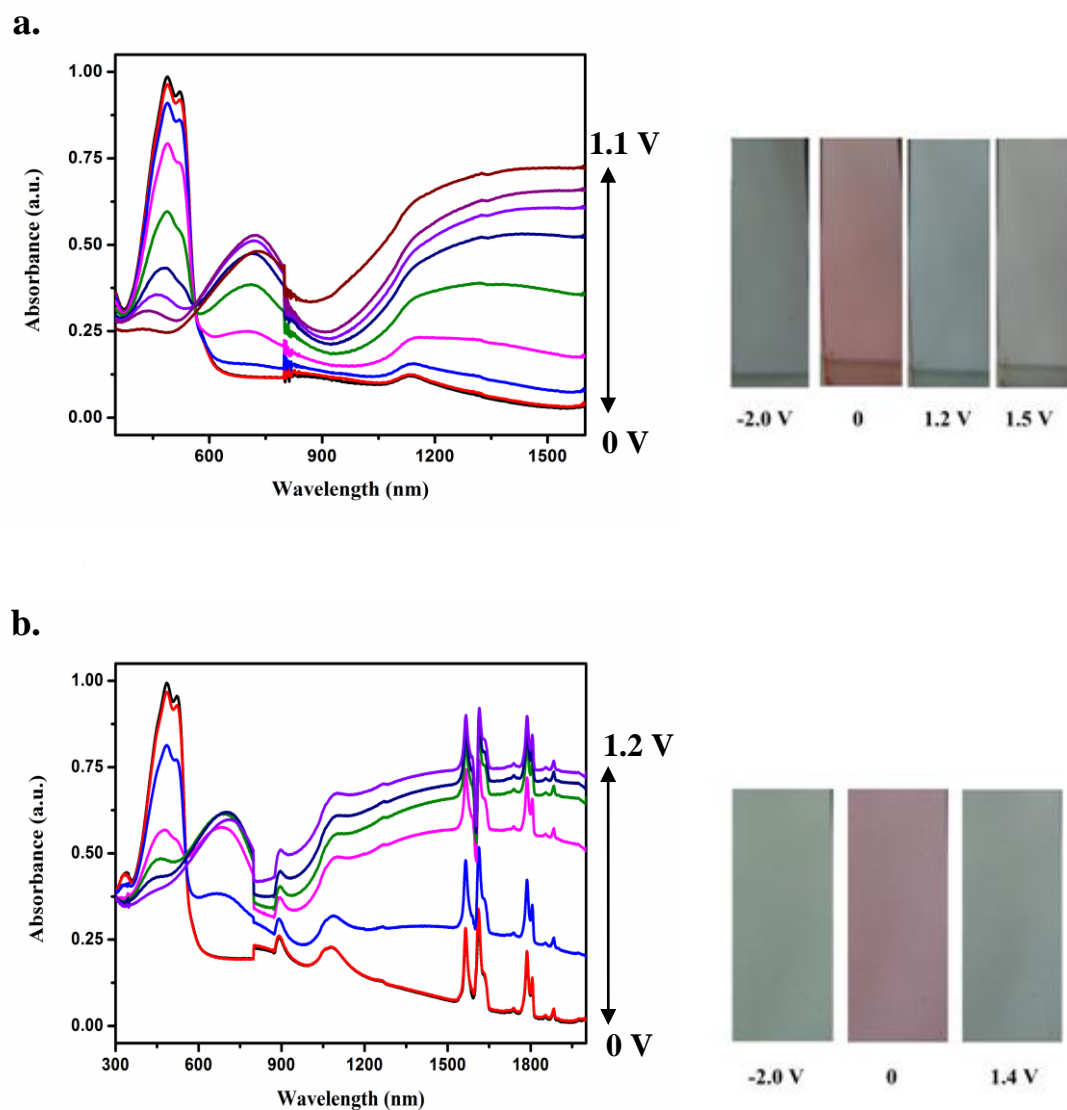


Figure 33. Spectroelectrochemical graphs and colors of (a) **P1** (b) **P2** at various applied potential

3.5. Kinetic Studies

The aim of the kinetic studies was to find out the percent transmittance changes and switching times of polymers between neutral and fully oxidized states. With this aim, maximum wavelengths of polymers were chosen and voltages were stepped between 0.0 V-1.1 V for P1 and 0.0 V-1.2 V for P2 in a determined time range. The

percent transmittance changes were determined by using UV-Vis-NIR spectrometer. Sensitivity of human eye was accepted as 95 % of full contrast. Therefore, percent transmittance changes were calculated based on this value. Switching times of **P1** was higher than **P2**. The reason of this might based on ion diffusion, dopant insertion, thickness and morphology of the film. Related graphs were shown in Figure 34. Optical contrasts were 25 % at 1500 nm and 15 % at 520 nm for **P1**. Similarly, they were 37 % at 1940 nm and 32 % at 490 nm for **P2** that were summarized in Table 5. Kinetic properties of polymers had better results at NIR region since polymers reached the quinoid feature. According to these results, **P2** is a good candidate with the lowest switching time and the highest optical contrast for NIR applications.

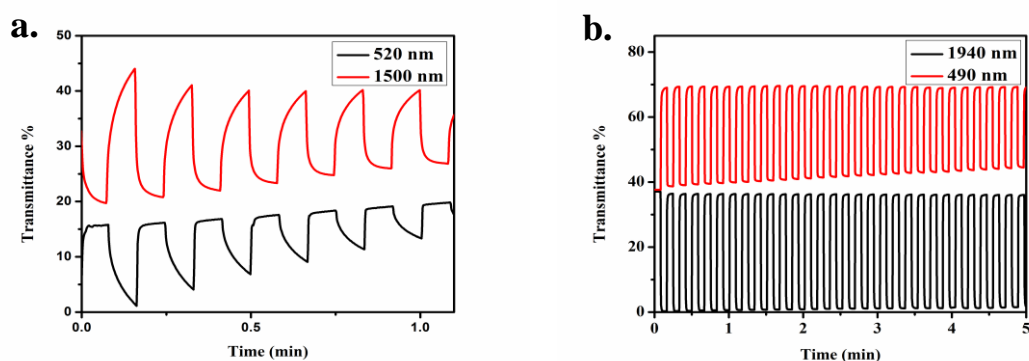


Figure 34. Percent transmittance changes of (a) **P1** and (b) **P2** in 0.1 M TBAPF₆ / ACN electrolyte solution at maximum wavelengths of polymers

Table 5. Optical contrast and switching time values of **P1** and **P2**

	Wavelength (nm)	Switching time (s)	Optical Contrast (% T)
P1	1500 nm	3.9	25
	520 nm	1.2	15
P2	1940 nm	0.8	37
	490 nm	0.9	32

3.6. OLED Applications

Photoluminescence (PL) properties of polymers were investigated as depicted in Figure 35. Maximum absorption wavelengths of polymers were selected as excitation wavelengths. The emission wavelengths were centered at 620 nm for **P1** and 631 nm for **P2** in their film form. In chloroform, emission wavelengths were centered at 590 nm for **P1** and 582 nm for **P2**, respectively. According to PL graphs, the thin film spectra of **P1** and **P2** were red shifted according to their solution spectra. The reasons of red shift emission were descending conformational freedom, interaction between polymer and solvent and aggregation tendency in thin film form [76-78]. Emission color was observed as orange for both polymers.

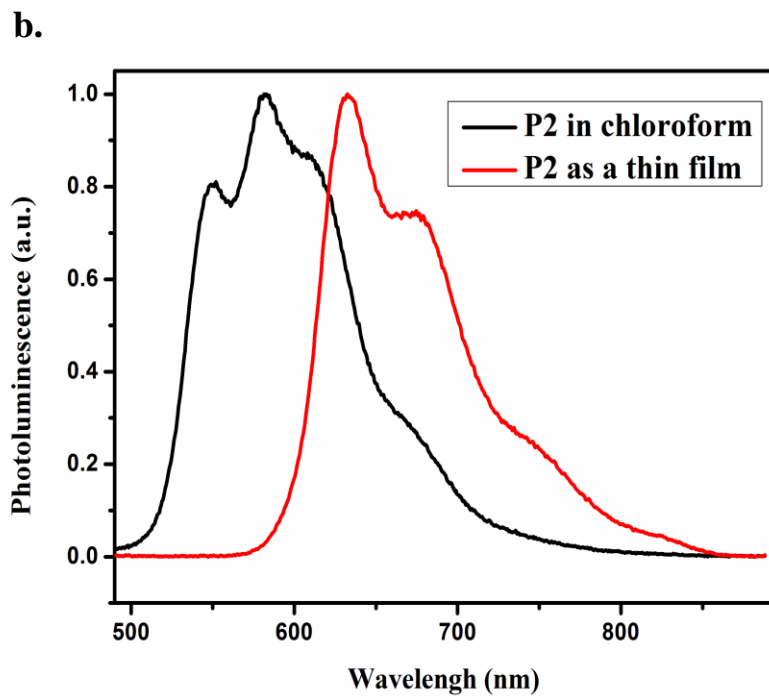
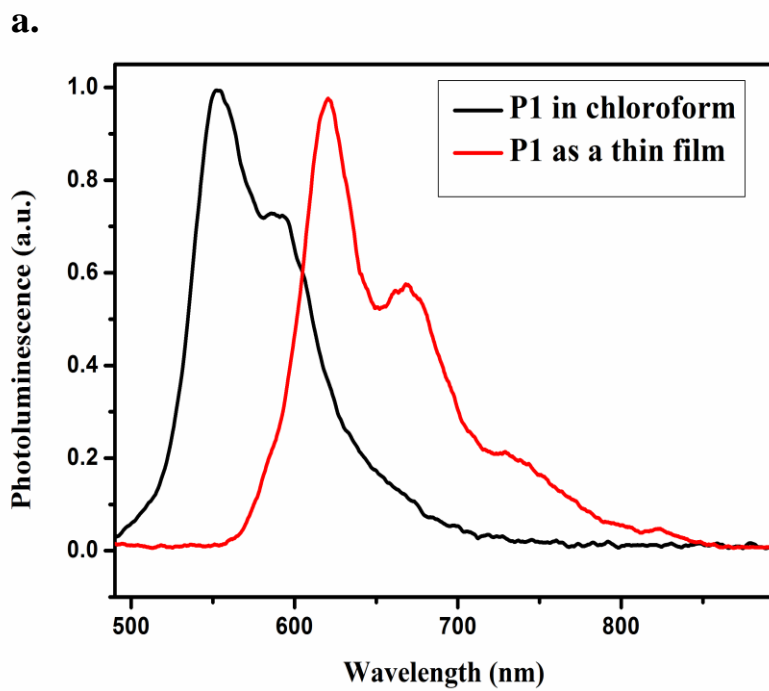


Figure 35. The photoluminescence spectra of (a) **P1** and (b) **P2** in the thin film and in chloroform solution

The ITO/PEDOT:PSS/polymers/LiF/Al configurations were constructed for PLEDs. Then, their device characterizations were investigated and related energy diagram was indicated in Figure 36.

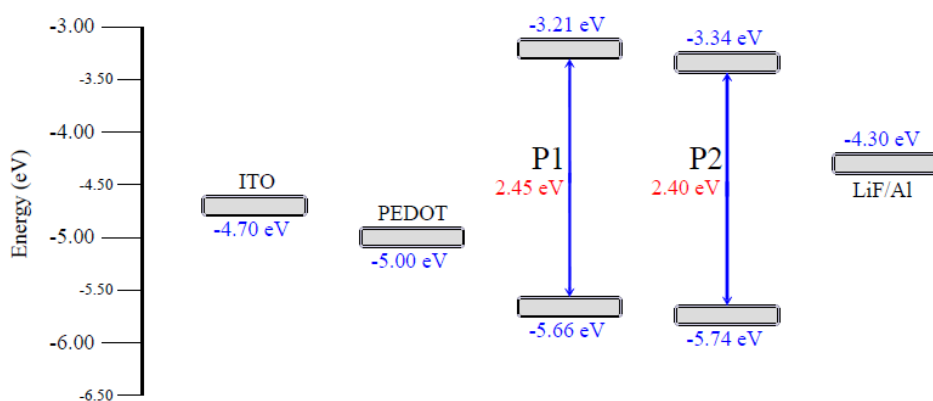


Figure 36. The energy levels of materials used in OLED device fabrication

Current density and luminance properties of devices were investigated as depicted in Figure 37. Turn on voltages of devices were determined as 5V for **P1** based device and 4V for **P2** based device. Lower turn on voltages led to lower power consumption and better durability. Injection barrier of electrons and holes was higher for **P1** hence transportation of charge carriers might be rather difficult. Therefore, turn on voltage of **P1** based OLED device was higher than **P2** based OLED device. Luminance-voltage characteristics were investigated and luminance values were determined as 6608 cd/m² for **P1** and 2540 cd/m² luminance for **P2**. Luminous efficiencies were 0.95 cd/A for **P1** at 8.0 V and 0.27 cd/A for **P2** at 9.5 V, respectively. EL properties of polymers were investigated depicted in Figure 38.

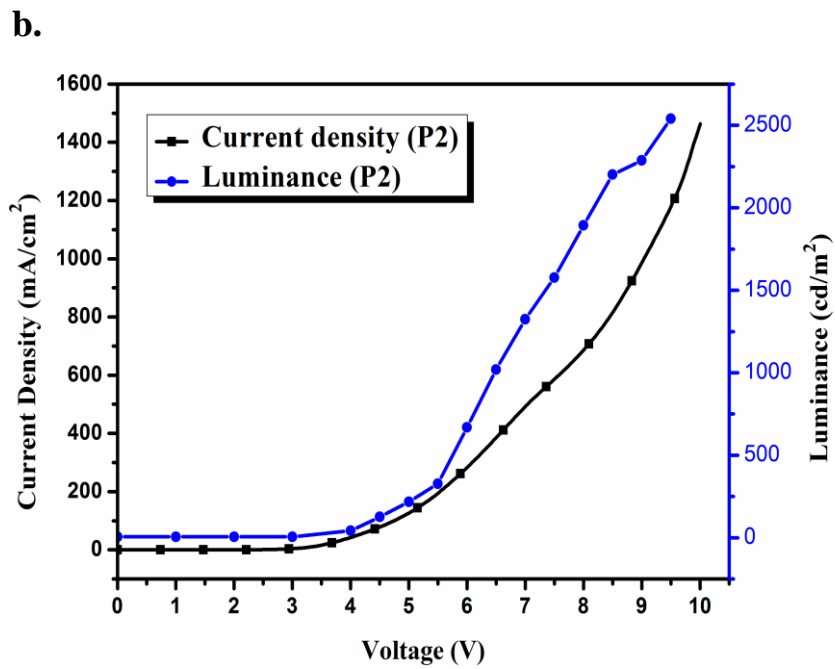
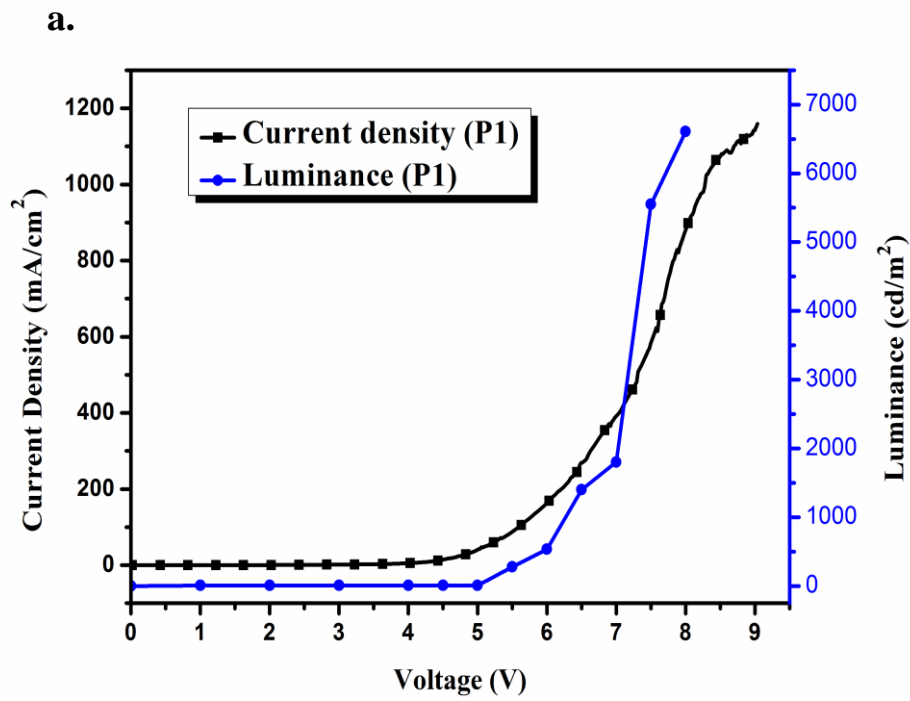


Figure 37. Current density-voltage-luminance characteristics of the (a) ITO/PEDOT:PSS/**P1**/LiF/Al device and (b) ITO/PEDOT:PSS/**P2**/LiF/Al device

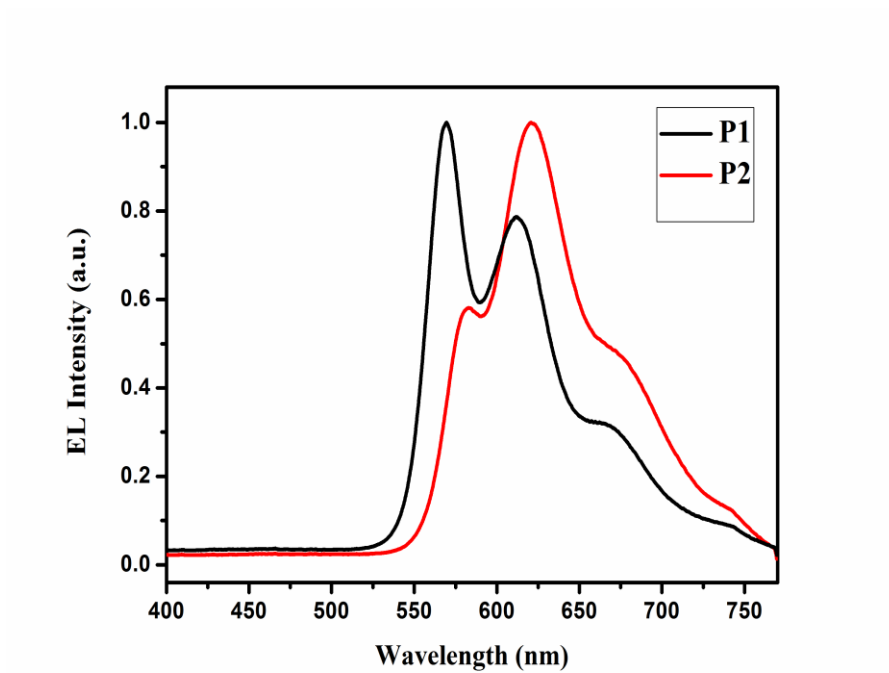


Figure 38. Electroluminescence spectra of (a) ITO/PEDOT:PSS/**P1**/LiF/Al device and (b) ITO/PEDOT:PSS/**P2**/LiF/Al device

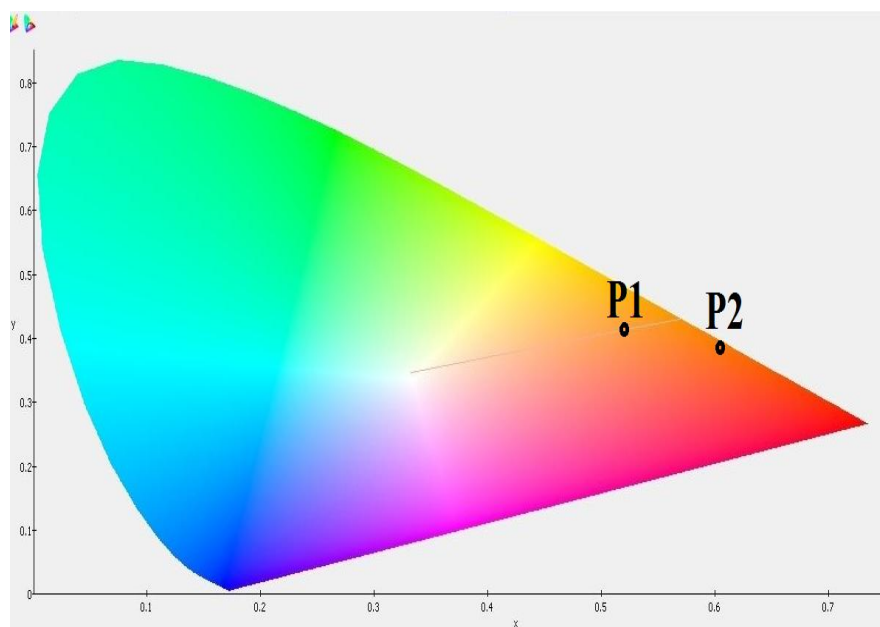


Figure 39. The CIE chromaticity diagram of ITO/PEDOT:PSS/polymers/LiF/Al

In Figure 39, the CIE Chromaticity coordinates of devices are determined as $x=0.5197$, $y=0.4123$ for **P1** and $x=0.6115$, $y=0.3810$ for **P2**. P1 based device was nearly close to the pure orange color ($x=0.5197$, $y=0.4214$). The views of constructed devices were depicted in Figure 40.

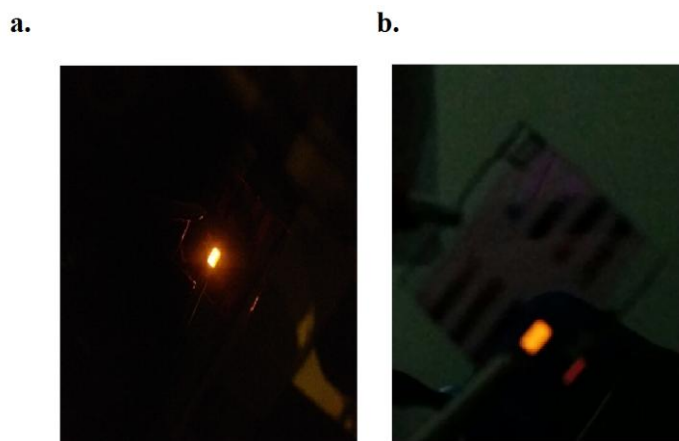


Figure 40. Photographs of an OLED device containing (a) **P1** and (b) **P2**

3.7.Solar Cell Applications

Bulk heterojunction solar cell applications of ITO/PEDOT:PSS/**P2**:PC₇₁BM/LiF/Al device was investigated with AM 1.5 G illumination. The energy level diagram was depicted in Figure 41.

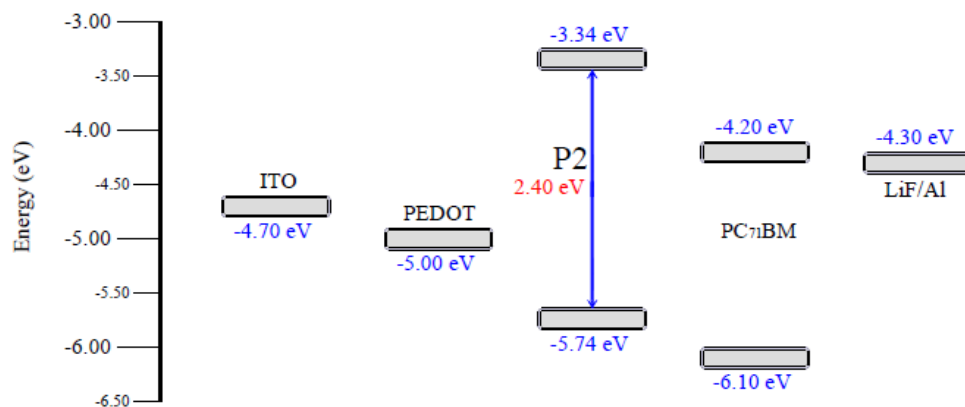


Figure 41. The energy levels of materials used in OSC device fabrication

Current density-voltage (J - V) properties of **P2** based OSC devices were investigated using different **P2**:PC₇₁BM weight ratios as indicated in Figure 42. PCE (η) values were calculated as 0.78, 0.97, 1.75, 1.60 for 1:1, 1:2 and 1:3 and 1:4 (w/w) **P2**:PC₇₁BM weight ratios, respectively and photovoltaic parameters were summarized in Table 6. It is noteworthy to state that the best performance of **P2** device indicated a V_{oc} of 0.86 V, a J_{sc} of 4.32 mA/cm², a fill factor (FF) of 47.0 %, and a PCE of 1.75 %. Although PCE increased with 1:3 (w/w) **P2**:PC₇₁BM ratio, PCE decreased to 1.60 % at 1:4 (w/w) **P2**:PC₇₁BM ratio. The reason of decreasing PCE from 1:3 to 1:4 **P2**:PC₇₁BM ratio was a low J_{sc} due to disrupted interaction between polymer and PC₇₁BM.

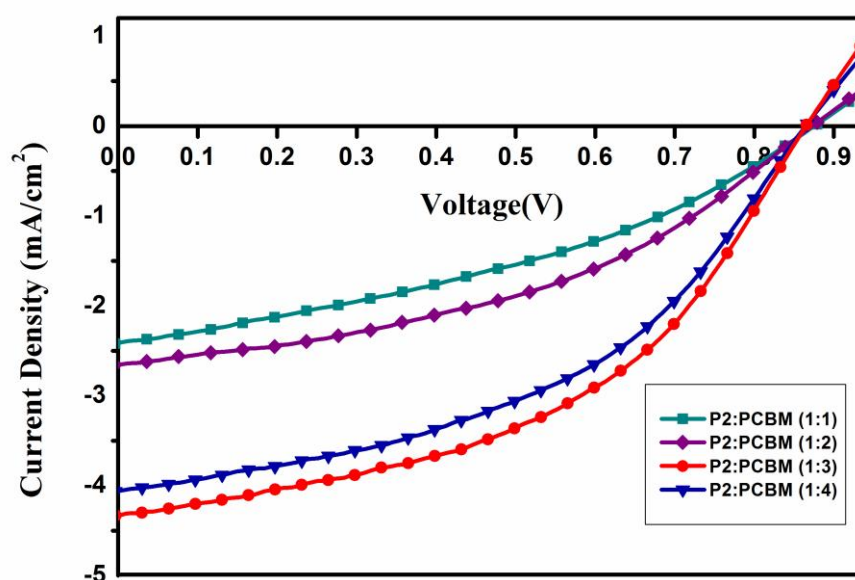


Figure 42. Light J - V characterization of the polymer solar cells made from **P2** blended with PC₇₁BM

The maximum incident photon to current efficiency (IPCE) was performed in order to investigate how much photon could be converted to current and related graph was depicted in Figure 43. With this aim, monochromatic light was used between 300 nm and 1000 nm and 20 % IPCE was measured for **P2**:PC₇₁BM (1:3 w/w) based device.

Solvent annealing, thermal annealing, usage of additives, morphology of active layer and thickness optimizations will be performed in order to improve the efficiency [67].

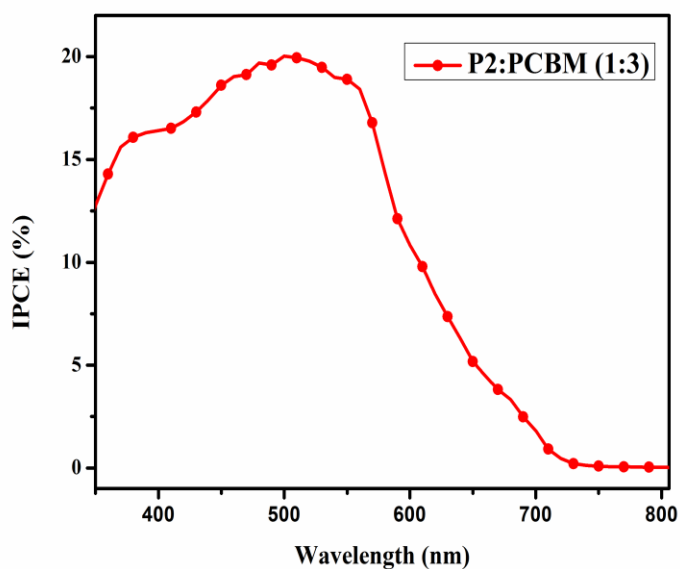


Figure 43. IPCE curve of photovoltaic device using **P2** donor blended with PC₇₁BM

Table 6. Photovoltaic properties of **P2:PC₇₁BM** solar cells with different donor-acceptor weight ratio

	J_{sc} (mA/cm ²)	V_{oc} (V)	J_{mp} (mA/cm ²)	V_{mp} (V)	FF (%)	η (%)
1:1	2.42	0.87	1.42	0.55	37	0.78
1:2	2.65	0.87	1.73	0.56	42	0.97
1:3	4.32	0.86	2.98	0.59	47	1.75
1:4	4.06	0.86	2.72	0.59	46	1.60

CHAPTER 4

CONCLUSION

4-(5-(7-Methyl-9,9-dioctyl-9H-fluoren-2-yl)-7-(5-methylselenophen-2-yl)-2-(2-octyl dodecyl)-2H-benzo[d][1,2,3] triazole (**P1**) and 9-(heptadecan-9-yl)-2-methyl-7-(5-(7-(5-methylselenophen-2-yl)-2-(2-octyldodecyl)-2H-benzo[d][1,2,3]triazol-4-yl)selenophen-2-yl)-9H-carbazole (**P2**) were synthesized by using Suzuki coupling reactions. Electrochemical properties of polymers were investigated by CV and electronic band gap was calculated as 2.45 eV for **P1** and 2.40 eV for **P2**. Both polymers have suitable electronic band gaps for optoelectronic applications. According to kinetic studies, switching time and optical contrast were investigated and especially **P2** is a good candidate with the lowest switching time and highest optical contrast for NIR applications. Maximum luminance was 6608 cd/m² at 7.5 V working voltage for **P1** and 2540 cd/m² at 9.5 V working electrode for **P2**. Luminous efficiencies were 0.95 cd/A for **P1** at 8.0 V and 0.27 cd/A for **P2** at 9.5 V. According to CIE Chromaticity diagram, the colors were observed as almost pure orange. Different amounts of PC₇₁BM were blended with **P2** and the best performance of **P2** based device yielded a V_{oc} of 0.86 V, a J_{sc} of 4.32 mA/cm², a fill factor (FF) of 47.0 %, and a PCE of 1.75

%. The study proved that polymers are promising candidates for optoelectronic applications.

REFERENCES

- [1] C. W. Tang, S. A. Vanslyke, and C. H. Chen, "Electroluminescence of doped organic thin films," *J. Appl. Phys.*, vol. 65, no. 9, pp. 3610–3616, 1989.
- [2] R. H. Partridge, "Electroluminescence from polyvinylcarbazole films: 3. Electroluminescent devices," *Polymer (Guildf.)*, vol. 24, no. 6, pp. 748–754, 1983.
- [3] D. Fyfe, "LED Technology: Organic displays come of age," *Nat. Photonics*, vol. 3, no. 8, pp. 453–455, 2009.
- [4] B. W. D'Andrade and S. R. Forrest, "White Organic Light-Emitting Devices for Solid-State Lighting," *Adv. Mater.*, vol. 16, no. 18, pp. 1585–1595, 2004.
- [5] C.E.Fritts, "On a new form of selenium photocell.," *Am. J. Sci.*, vol. 26, pp. 465-468, 1883.
- [6] A. E. Becquerel, "Memoire sur les effets électriques produits sous l'influence des rayons solaires," *Compt. Rend. Acad. Sci.*, vol. 9, no. 145, pp. 561–567, 1839.
- [7] D.M.Chopin, C.S.Fuller, G.L.Pearson," A new silicon p-n junction photocell for converting solar radiation into electrical power," *J. Appl. Phys.*, vol. 25, pp. 676-679,1954.
- [8] D. E. Carlson and C. R. Wronski, "Amorphous silicon solar cell," *Appl. Phys. Lett.*, vol. 28, no. 11, pp. 671–673, 1976.
- [9] F. So, J. Kido, and P. Burrows, "Organic Light- Emitting Devices for Solid-State Lighting Introduction : The Potential for," *MRS Bull.*, vol. 33, pp. 663–669, 2008.
- [10] J.-H. Jou, P.-H. Wu, C.-H. Lin, M.-H. Wu, Y.-C. Chou, H.-C. Wang, and S.-M. Shen, "Highly efficient orange-red organic light-emitting diode using double emissive layers with stepwise energy-level architecture," *J. Mater. Chem.*, vol. 20, p. 8464, 2010.
- [11] L. Dai, "Conducting Polymers," in *Intelligent Macromolecules for Smart Devices*, London: Springer-Verlag, pp. 41–80, 2003.
- [12] R. H. Friend, R. W. Gymer, A. B. Holmes, J. H. Burroughes, R. N. Marks, C. Taliani, D. D. C. Bradley, D. A. Dos Santos, J. L. Bredas, M. Logdlund, and W. R. Salaneck, "Electroluminescence in conjugated polymers," *Nature*, vol.

- 397, pp. 121–128, 1999.
- [13] G. Horowitz, “Organic Field-Effect Transistors,” *Adv. Mater.*, vol. 10, no. 5, pp. 365–377, 1998.
- [14] A. Heller, “Electrical Wiring of Redox Enzymes,” *Acc. Chem. Res.*, vol. 23, pp. 128–134, 1990.
- [15] S. Gu, H. Neugebauer, and N. S. Sariciftci, “Conjugated Polymer-Based Organic Solar Cells,” pp. 1324–1338, 2007.
- [16] J. Shinar, *Organic light-emitting devices: a survey*. USA: Springer-Verlag, 2004.
- [17] J. G. Drobny, *Polymers for Electricity and Electronics: Materials, Properties, and Applications*, John Wiley Sons, Inc., New York, 2012.
- [18] W. Kern, *Handbook of semiconductor wafer*, Noyes Pub., pp. 455–475, 1993.
- [19] W.A. Gazotti, A.E. Nogueira, E.M. Girotto, L.D. P. Condutores, I. De Quimica, U. E. De, S. Paulo, L. Micaroni, D. De Quimica, U. Federal, M. Martini, L. De Cristalografia, D. D. F. Aplicada, I. De Fisica, U. D. S. Paulo, S. Paulo, S. Neves, M. De Paoli, and L. D. M. Eletroativos, *Optical Devices Based on Conductive Polymers*, vol. 10, 2001.
- [20] G. B. Street, “Upon Doping,” vol. 30, no. 2, pp. 1023–1025, 1984.
- [21] J. Bredas and G. Street, “Polarons, bipolarons, and solitons in conducting polymers,” *Acc. Chem. Res.*, vol. 1305, no. 4, pp. 309–315, 1985.
- [22] A. A. Argun, P. H. Aubert, B. C. Thompson, I. Schwendeman, C. L. Gaupp, J. Hwang, N. J. Pinto, D. B. Tanner, A. G. MacDiarmid, and J. R. Reynolds, “Multicolored electrochromism in polymers: Structures and devices,” *Chem. Mater.*, vol. 16, no. 23, pp. 4401–4412, 2004.
- [23] T. Moore, “Cyclometallated iridium-carbazole complexes for applications,” PHD Thesis, University of Durham, 2008.
- [24] U. Mitschke, P. Baulerle, “Electroluminescence of conjugated aromatic polymers in organic light emitting diodes,” *J. Mater. Chem.*, vol. 10, no. 7, pp. 1471–1507, 2005.
- [25] C. Kittel, *Introduction to Solid State Physics*, John Wiley Sons, Inc., New York, vol. 8, 2004.

- [26] B.Herman, J. R. Lakowicz, and D. B. Murphy, "Fluorescence Excitation and Emission Fundamentals," 2009.
- [27] B. Geffroy, P. L.Roy, and C. Prat, "Organic light-emitting diode (OLED) technology: Materials, devices and display technologies," *Polym. Int.*, vol. 55, no. 6, pp. 572–582, 2006.
- [28] P. T. C. So and C. Y. Dong, "Fluorescence Spectrophotometry," *Encycl. Life Sci.*, pp. 1–4, 2002.
- [29] C. Zhang, Y. S. Zhao, and J. Yao, "Organic composite nanomaterials: energy transfers and tunable luminescent behaviors," *New J. Chem.*, vol. 35, no. 5, p. 973, 2011.
- [30] J. Heine and K. Müller-Buschbaum, "Engineering metal-based luminescence in coordination polymers and metal–organic frameworks," *Chem. Soc. Rev.*, vol. 42, no. 24, p. 9232, 2013.
- [31] C. B. Murphy, Y. Zhang, T. Troxler, V. Ferry, J. J. Martin, and W. E. Jones, "Probing Forster and Dexter Energy-Transfer Mechanisms in Fluorescent Conjugated Polymer Chemosensors," *J. Chem. B*, vol. 17, no. 108, pp. 1537–1543, 2004.
- [32] Y.C. Chen, G.S. Huang, C.C. Hsiao, and S.A. Chen, "High triplet energy polymer as host for electrophosphorescence with high efficiency.," *J. Am. Chem. Soc.*, vol. 128, no. 26, pp. 8549–58, 2006.
- [33] Y. Tao, C. Yang, and J. Qin, "Organic host materials for phosphorescent organic light-emitting diodes," *Chem. Soc. Rev.*, vol. 40, no. 5, p. 2943, 2011.
- [34] S. H. Lin, W. Z. Xiao, and W. Dietz, "Generalized Forster-Dexter theory of photoinduced intramolecular energy transfer," *Phys. Rev. E*, vol. 47, no. 5, pp. 3698–3706, 1993.
- [35] M. Pfeiffer, K. Leo, X. Zhou, J. S. Huang, M. Hofmann, A. Werner, and J. Blochwitz-Nimoth, "Doped organic semiconductors: Physics and application in light emitting diodes," *Org. Electron.*, vol. 4, no. 2–3, p. 89, 2003.
- [36] P. E. Burrows, G. Gu, V. Bulović, Z. Shen, S. R. Forrest, and M. E. Thompson, "Achieving full-color organic light-emitting devices for lightweight, flat-panel displays," *IEEE Trans. Electron Devices*, vol. 44, no. 8, pp. 1188–1203, 1997.
- [37] C. Summitt, "OLED Fabrication for Use in Display Systems," PHD Thesis,

University of Arizona, Tucson, p. 9, 2006.

- [38] V. Michael, "Fabrication of OLED on FTO and ITO coated Substrates By Emerging Technologies Research Centre ," vol. 11287888, no. September, 2012.
- [39] R. Schlaf, H. Murata, and Z. . Kafafi, "Work function measurements on indium tin oxide films," *J. Electron Spectros. Relat. Phenomena*, vol. 120, no. 1–3, pp. 149–154, 2001.
- [40] A. Cirpan and F. E. Karasz, "Indium tin oxide nanoparticles as anode for light-emitting diodes," *J. Appl. Polym. Sci.*, vol. 99, no. 6, pp. 3125–3129, 2006.
- [41] J. H. Cook, H. A. Al-Attar, and A. P. Monkman, "Effect of PEDOT-PSS resistivity and work function on PLED performance," *Org. Electron. physics, Mater. Appl.*, vol. 15, no. 1, pp. 245–250, 2014.
- [42] M. Stssel, J. Staudigel, F. Steuber, J. Simmerer, and A. Winnacker, "Impact of the aathode metal work function on the performance of vacuum-deposited organic light emitting devices," *Appl. Phys. A - Mater.*, vol. 390, pp. 387–390, 1999.
- [43] S. E. Shaheen, G. E. Jabbour, M. M. Morrell, Y. Kawabe, B. Kippelen, N. Peyghambarian, M. F. Nabor, R. Schlaf, E. a Mash, and N. R. Armstrong, "Bright blue organic light-emitting diode with improved color purity using a LiF/Al cathode," *J. Appl. Phys.*, vol. 84, no. 1998, pp. 2324–2327, 1998.
- [44] J. Shinar, "Organic electronics: Organic thin-film magnetometers," *Nat. Mater.*, vol. 11, no. 8, pp. 663–664, 2012.
- [45] A. Islam, M. Rabbani, M. H. Bappy, M. A. R. Miah, and N. Sakib, "A review on fabrication process of organic light emitting diodes," *2013 Int. Conf. Informatics, Electron. Vis.*, pp. 1–5, 2013.
- [46] IPCC, "Climate change 2007: the physical science basis," *Intergov. Panel Clim. Chang.*, vol. 446, no. 7137, pp. 727–8, 2007.
- [47] E. A. Thomsen, "Characterisation of materials for organic photovoltaics," PHD Thesis, University of St. Andrews, 2008.
- [48] S.M.Sze, K. K. Ng, "*Physics of semiconductor devices*," John Wiley Sons, Inc., NewYork, vol.3, pp. 293-337, 2007.
- [49] T. Markvart, A.Mcevoy, L. Castañer, A.Martı, L.Lugue, "*Books about solar cells, photovoltaic systems, and applications*," Elseiver Ltd., pp. 1185-1188,

2003.

- [50] M. Green, "Solar Cells- Operating Principles, Technology and System Applications," *Englewood Cliffs, NJ, Prentice-Hall, Inc.*, pp. 1–39, 1982.
- [51] N. K. Jangid, N. P. Singh Chauhan, K. Meghwal, and P. B. Punjabi, "Conducting polymers and their applications," *Res. J. Pharm. Biol. Chem. Sci.*, vol. 5, no. 3, pp. 383–412, 2014.
- [52] H. Hoppe and N. Sariciftci, "Organic solar cells: An overview," *J. Mater. Res.*, vol. 19, no. 07, pp. 1924–1945, 2004.
- [53] M. S. AlSalhi, J. Alam, L. A. Dass, and M. Raja, "Recent Advances in Conjugated Polymers for Light Emitting Devices," *Int. J. Mol. Sci.*, vol. 12, no. 12, pp. 2036–2054, 2011.
- [54] G. H. Gelinck, J. M. Warman, M. Remmers, and D. Neher, "Narrow-band emissions from conjugated-polymer films," *Chem. Phys. Lett.*, vol. 265, no. 3–5, pp. 320–326, 1997.
- [55] E. E. Havinga, W. ten Hoeve, and H. Wynberg, "A new class of small band gap organic polymer conductors," *Polym. Bull.*, vol. 29, no. 1–2, pp. 119–126, 1992.
- [56] C. J. Brabec, S. Gowrisanker, J. J. M. Halls, D. Laird, S. Jia, and S. P. Williams, "Polymer-fullerene bulk-heterojunction solar cells," *Adv. Mater.*, vol. 22, no. 34, pp. 3839–3856, 2010.
- [57] M. Kim, "Understanding Organic Photovoltaic Cells: Electrode, Nanostructure, Reliability, and Performance," *ProQuest*, pp. 1–115, 2009.
- [58] A. Hagfeldt, G. Boschloo, S. Licheng, K. Lars, and H. Pettersson, "Dye-sensitized solar cells," *Chem. Rev.*, vol. 110, no. 11, pp. 6595–6663, 2010.
- [59] R. Gómez and J. L. Segura, "Plastic Solar Cells: A Multidisciplinary Field To Construct Chemical Concepts from Current Research," *J. Chem. Educ.*, vol. 84, no. 2, p. 253, 2007.
- [60] N. C. Greenham, "Polymer solar cells," *Phil.Trans.R.Soc.A.*, vol. 371, p. 414–420, 2013.
- [61] M. Karakus, D. H. Apaydn, D. E. Yldz, L. Toppare, and A. Cirpan, "Benzotriazole and benzothiadiazole containing conjugated copolymers for organic solar cell applications," *Polymer (Guildf)*, vol. 53, no. 6, pp. 1198–1202, 2012.

- [62] C. Song, T. Sai-Wing, C. E. Small, J. R. Reynolds, and F. So, "Inverted Polymer Solar Cells," *Photonics Journal, IEEE*, vol. 4, no. 2, pp. 625–628, 2012.
- [63] A. Balan, D. Baran, G. Gunbas, A. Durmus, F. Ozyurt, and L. Toppare, "One polymer for all: benzotriazole containing donor-acceptor type polymer as a multi-purpose material," *Chem. Commun...*, no. 44, pp. 6768–6770, 2009.
- [64] Y. Wu, S. Hwang, H. Chen, M. Lee, W. Shen, and C. H. Chen, "Efficient white organic light emitting devices with dual emitting layers," vol. 488, pp. 265–269, 2005.
- [65] G. Kocak, "Polymer white light emitting diodes applications of benzotriazole and fluorene derivatives," M.Sc. Thesis, METU, 2015.
- [66] E. Kaya, A. Balan, D. Baran, A. Cirpan, and L. Toppare, "Electrochromic and optical studies of solution processable benzotriazole and fluorene containing copolymers," *Org. Electron. physics, Mater. Appl.*, vol. 12, no. 1, pp. 202–209, 2011.
- [67] E. Kaya, D. H. Apaydn, D. E. Yldz, L. Toppare, and A. Cirpan, "Solution processable benzotriazole and fluorene containing copolymers for photovoltaic applications," *Sol. Energ. Mat. Sol. C.*, vol. 99, pp. 321–326, 2012.
- [68] O. Erlik, N. A. Unlu, G. Hizalan, S. O. Hacioglu, S. Comez, E. D. Yildiz, L. Toppare, and A. Cirpan, "Silafuorene-Based Polymers for Electrochromic and Polymer Solar Cell Applications," *J. Polym. Sci. A Polym. Chem.*, pp. 1541–1547, 2015.
- [69] Z. Zhang and J. Wang, "Structures and properties of conjugated Donor–Acceptor copolymers for solar cell applications," *J. Mater. Chem.*, vol. 22, no. 10, p. 4178, 2012.
- [70] Z. Zhang, B. Peng, B. Liu, C. Pan, Y. Li, Y. He, K. Zhou, and Y. Zou, "Copolymers from benzodithiophene and benzotriazole: synthesis and photovoltaic applications," *Polym. Chem.*, vol. 1, no. 9, p. 1441, 2010.
- [71] B. A. D. Neto, A. M. Lapis, E. S. Junior, J. Dupont, "2,1,3-Benzothiadiazole and Derivatives: Synthesis, Properties, Reactions, and Applications in Light Technology of Small Molecules," *Eur.J.Org.Chem.*, vol.5, pp. 228-255, 2013.
- [72] A. Tanimoto, T. Yamamoto, "Nickel-2,2'-Bipyridyl and PalladiumTriphenylphosphine Complex Promoted Synthesis of New π -

Conjugated Poly(2-hexylbenzotriazole)s and Characterization of the Polymers. *Adv. Synth. Catal.*,” vol. 346, pp. 1818-1823, 2004.

- [73] K. Pilgram, M. Zupan, R. Skiles,” Bromination of 2,1,3benzothiadiazoles,” *Journal of Heterocyclic Chemistry*, vol.7, no. 3, pp. 629-633, 1970.
- [74] R. J. Mortimer, “Electrochromic materials.,” *Chem. Soc. Rev.*, vol. 26, no. 3, pp. 147–156, 1997.
- [75] A. R. Johnson, “White-Light Generation and OLED Lifetime Issues,” PHD Thesis, University of Michigan, 2008.
- [76] P. Schouwink, A. H. Schafer, C. Seidel, and H. Fuchs, “The influence of molecular aggregation on the device properties of organic light emitting diodes,” *Thin Solid Films*, pp. 163–168, 2000.
- [77] J. Lee, G. Klaemer, R. D. Miller, “Structure-property relationship for excimer formation in poly (alkylfluorene) derivatives,” *Synt. Met.*, vol. 101, p. 6779, 1999.
- [78] T. Q. Nguyen, I. B. Martini, J. Lui, B. J. Schwartz, “Controlling interchain interactions in conjugated polymers: The effects of chain morphology on exciton-exciton annihilation and aggregation in MEH-PPV films,” *J.Phys.Chem.B.*, vol. 104, no. 2, pp. 237–255, 2000.
- [79] N. S. Neghmouche and T. Lanez, “Calculation of electrochemical parameters starting from the polarization curves of ferrocene at glassy carbon electrode,” *Int. Lett. Chem. Phys. Astron.*, vol. 4, pp. 37–45, 2013.

APPENDICES

A. NMR DATA

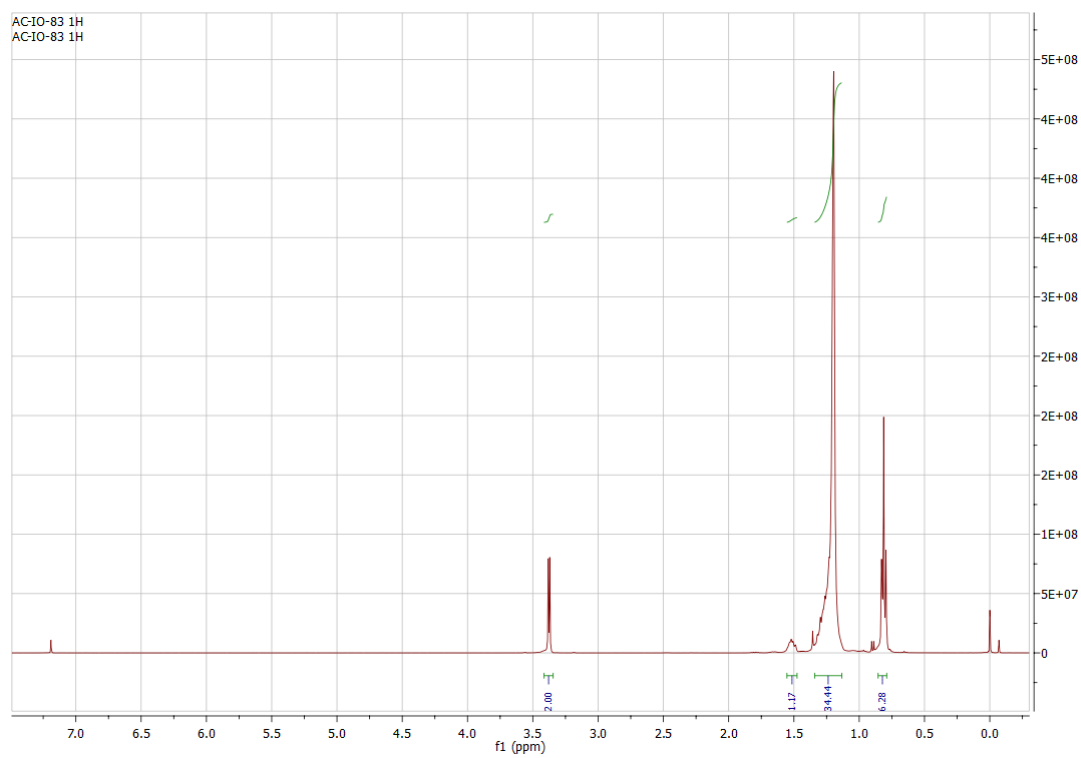


Figure 44. ^1H NMR of 9-(bromomethyl) nonadecane

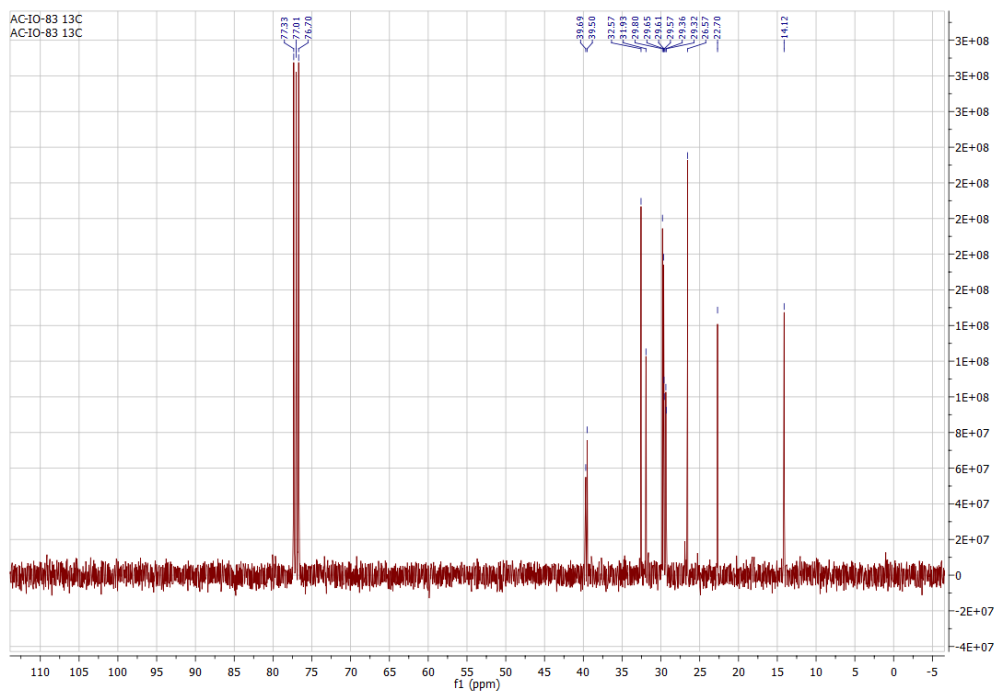


Figure 45. ^{13}C NMR 9-(bromomethyl) nonadecane

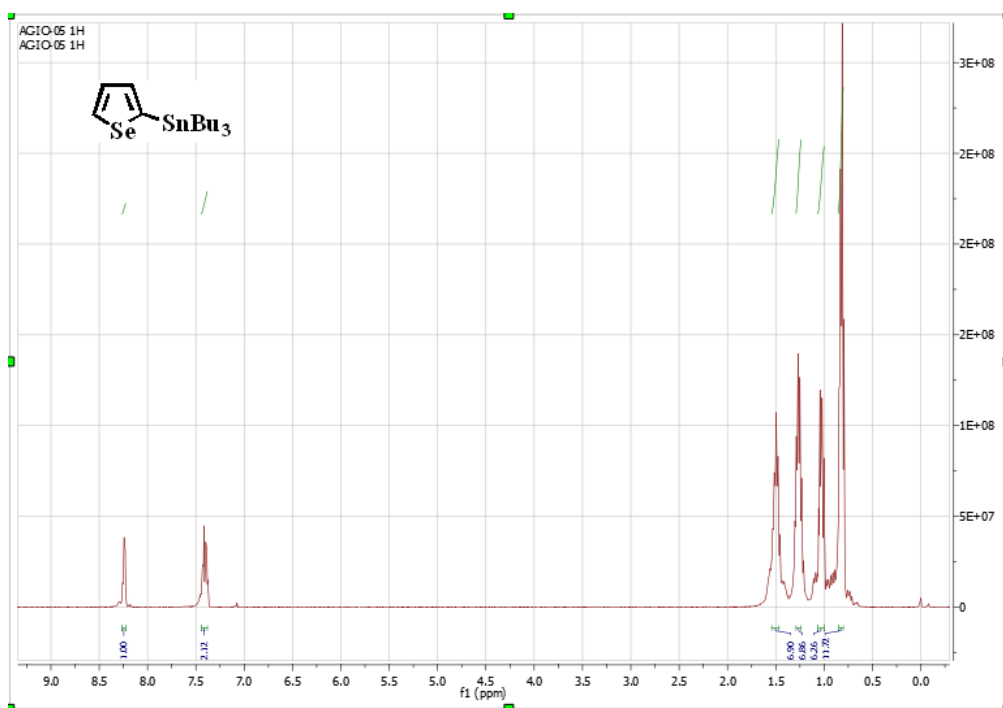


Figure 46. ^1H NMR of tributyl(selenophen-2-yl)stannane

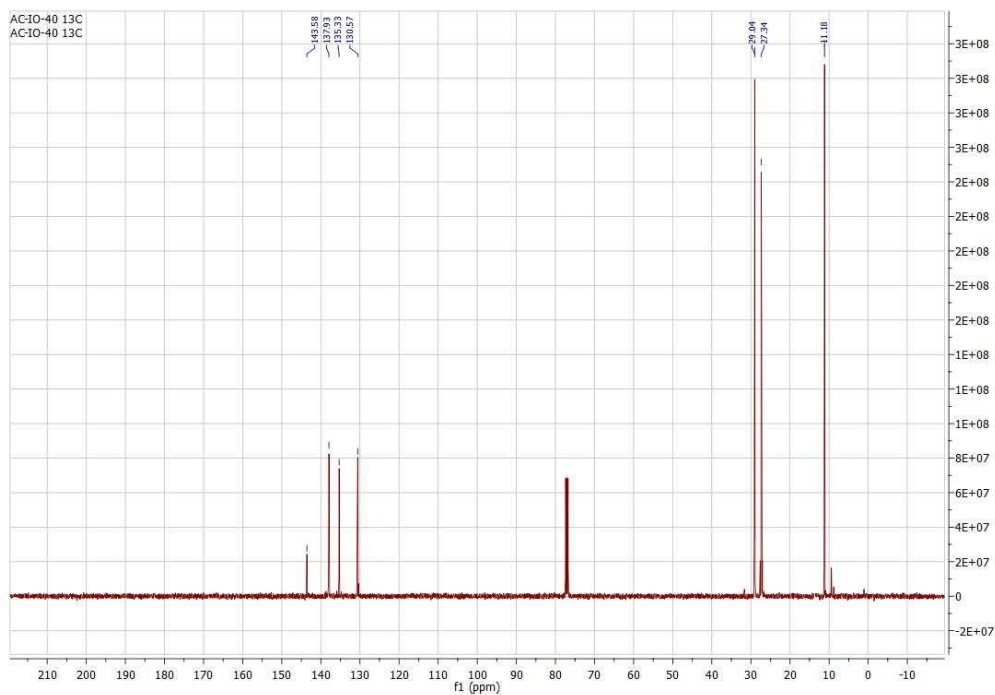


Figure 47. ^{13}C NMR of tributyl(selenophen-2-yl)stannane

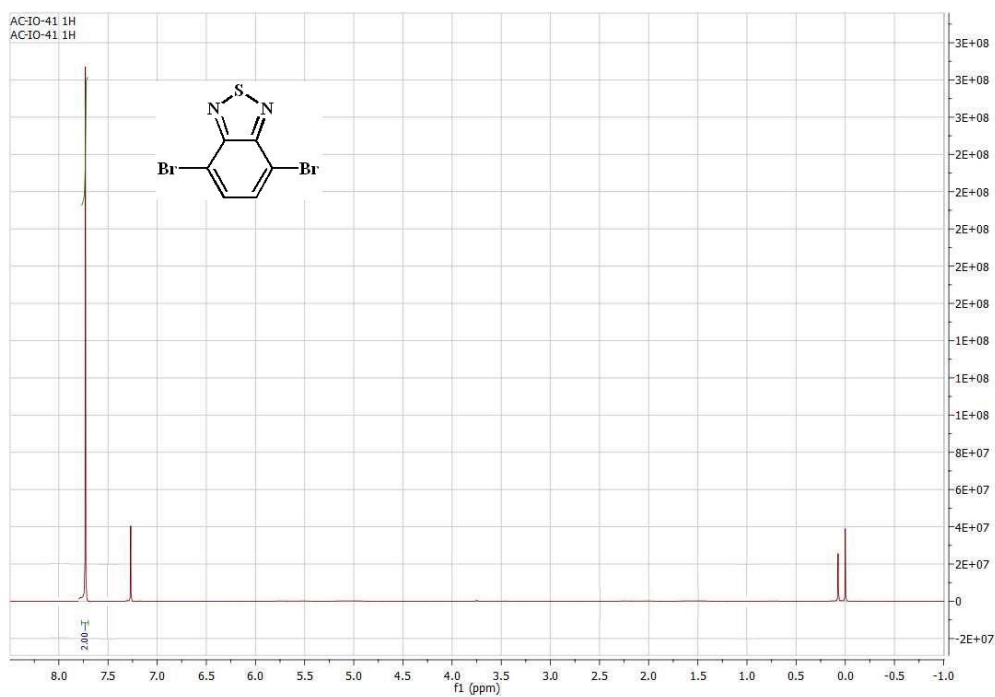


Figure 48. ^1H NMR of 4,7-dibromobenzo[c][1,2,5]thiadiazole

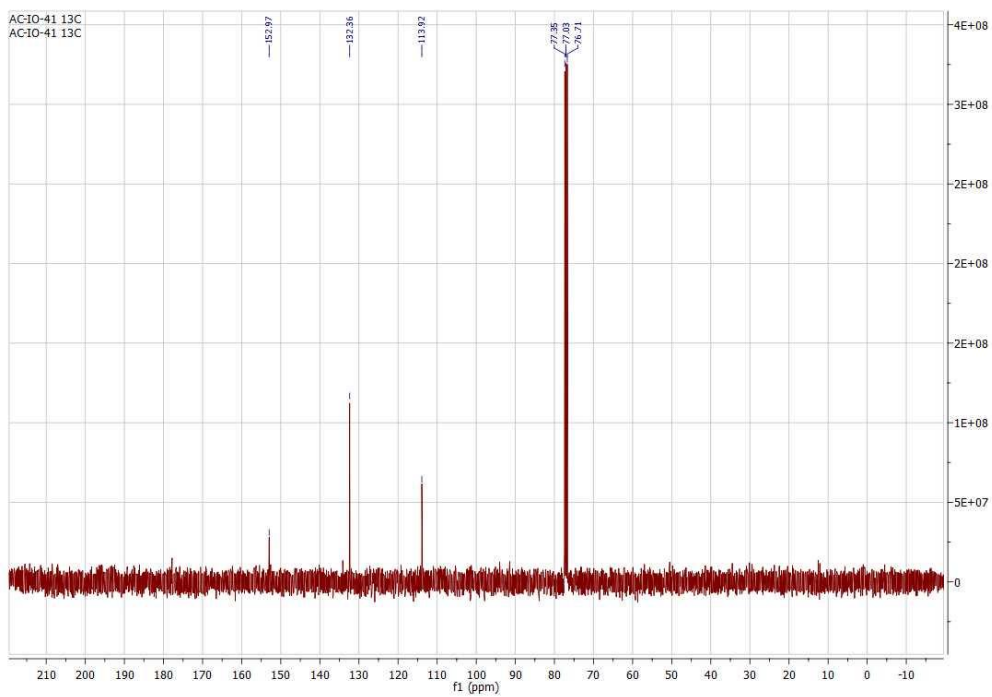


Figure 49. ^{13}C NMR of 4, 7-dibromobenzo[c][1,2,5] thiadiazole

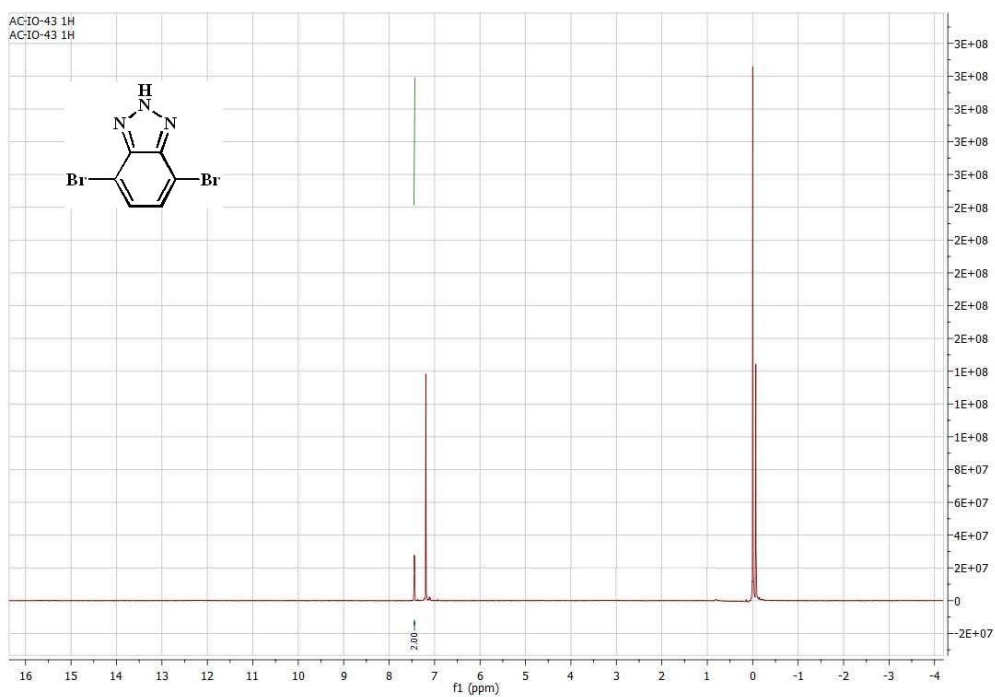


Figure 50. ^1H NMR of 4, 7-dibromo-2H-benzo[d][1,2,3]triazole

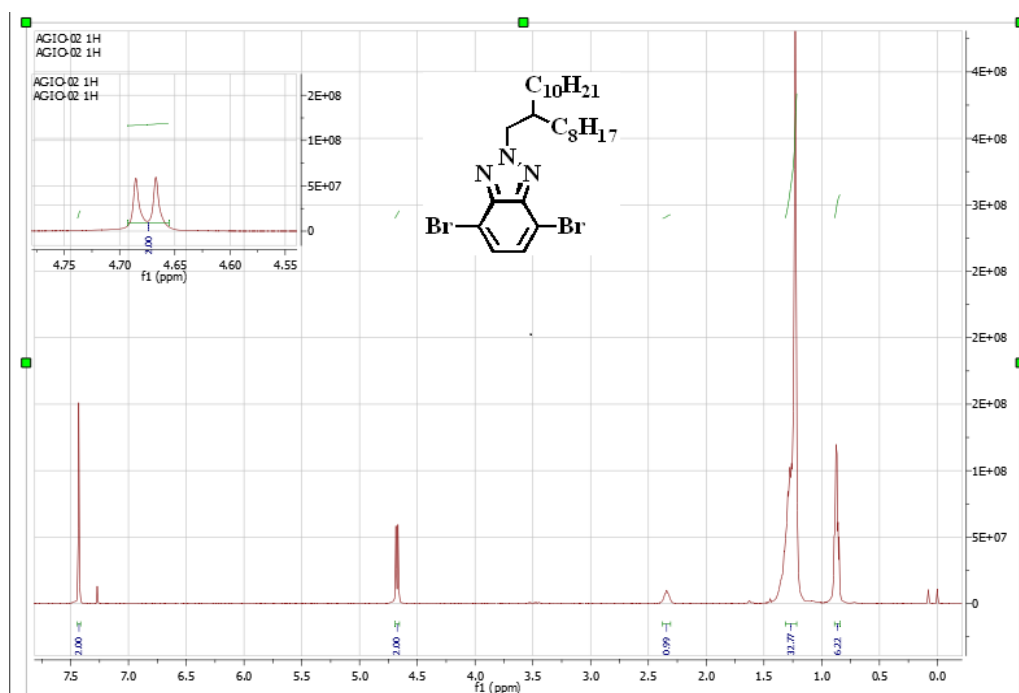


Figure 51. ^1H NMR of 4, 7-dibromo-2-(2-octyldodecyl) - 2H -benzo[d] [1, 2, 3] triazole

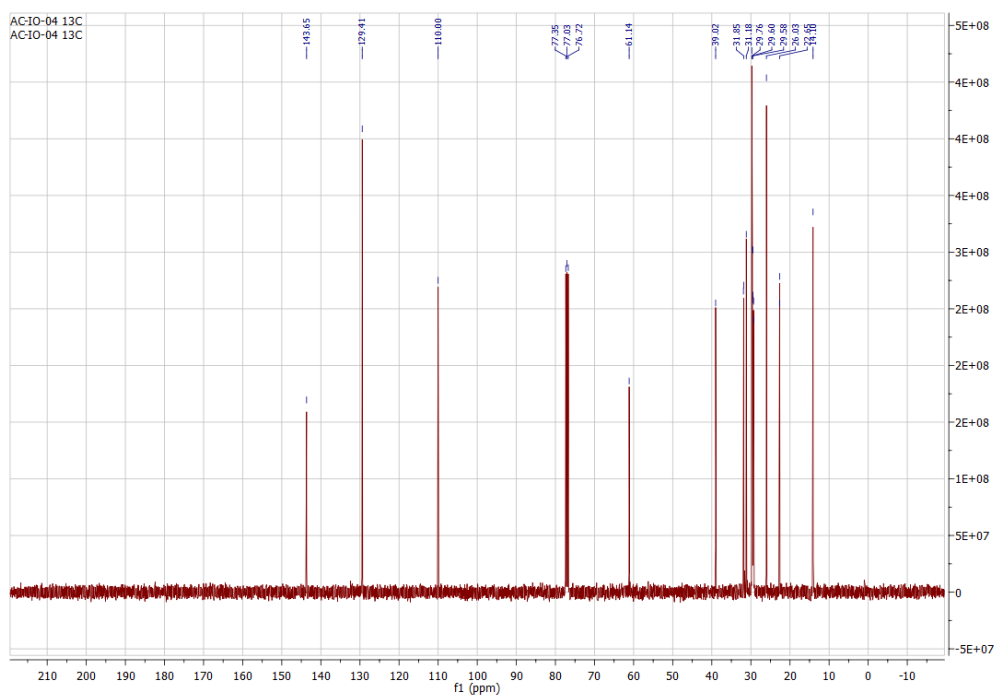


Figure 52. ^{13}C MNR of 4, 7-dibromo-2-(2-octyldodecyl) - 2H -benzo[d] [1, 2, 3] triazole

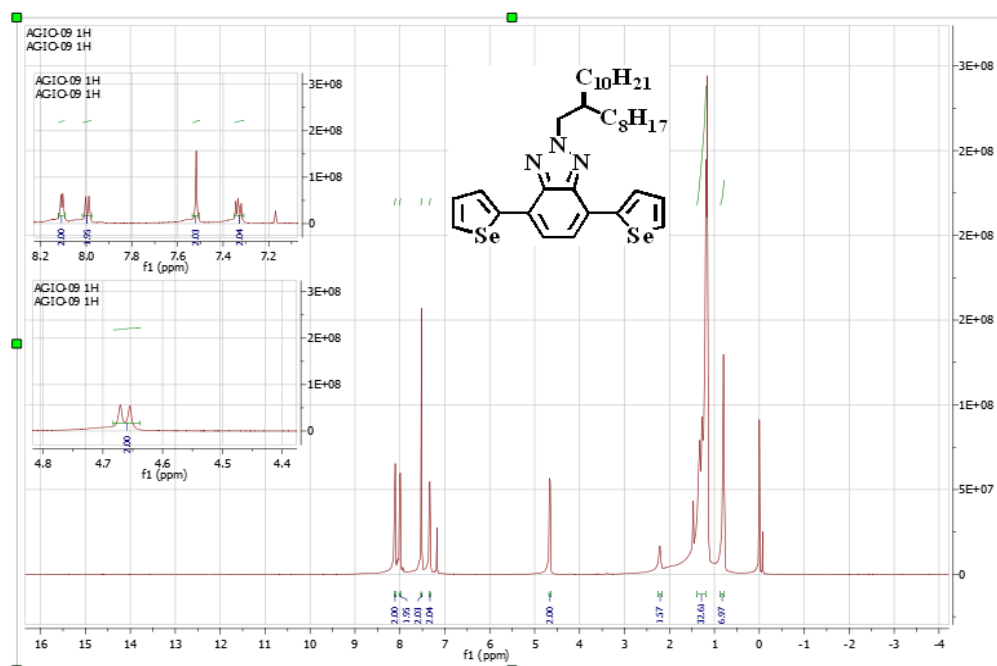


Figure 53. ^1H NMR of 2-(2-octyldodecyl)-4,7-di(selenophen-2-yl)-2H-benzotriazole

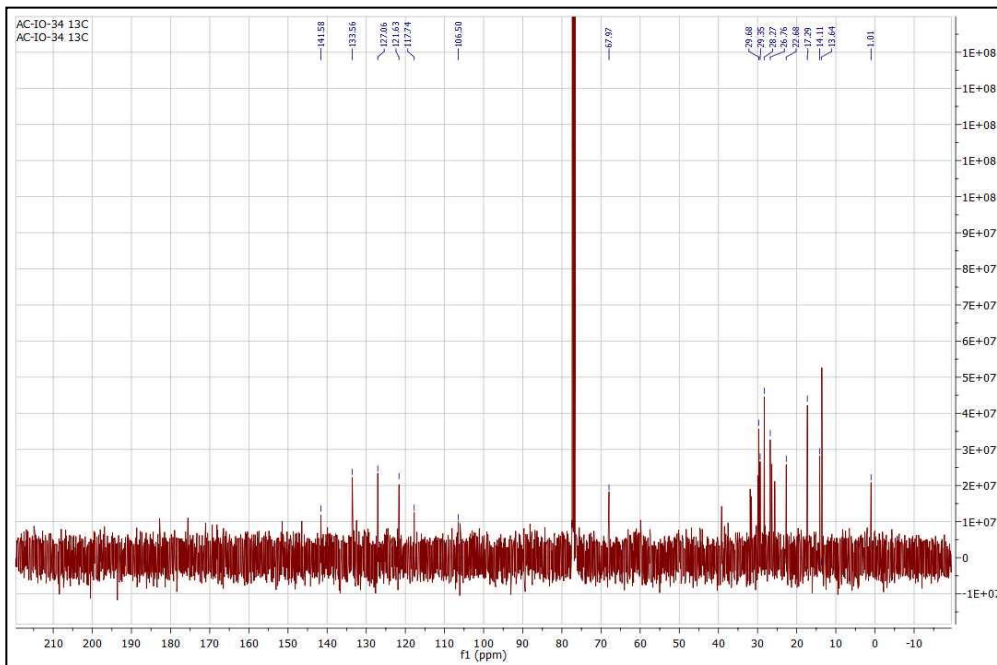


Figure 54. ^{13}C NMR of 2-(2-octyldodecyl)-4,7-di(selenophen-2-yl)-2H-benzotriazole

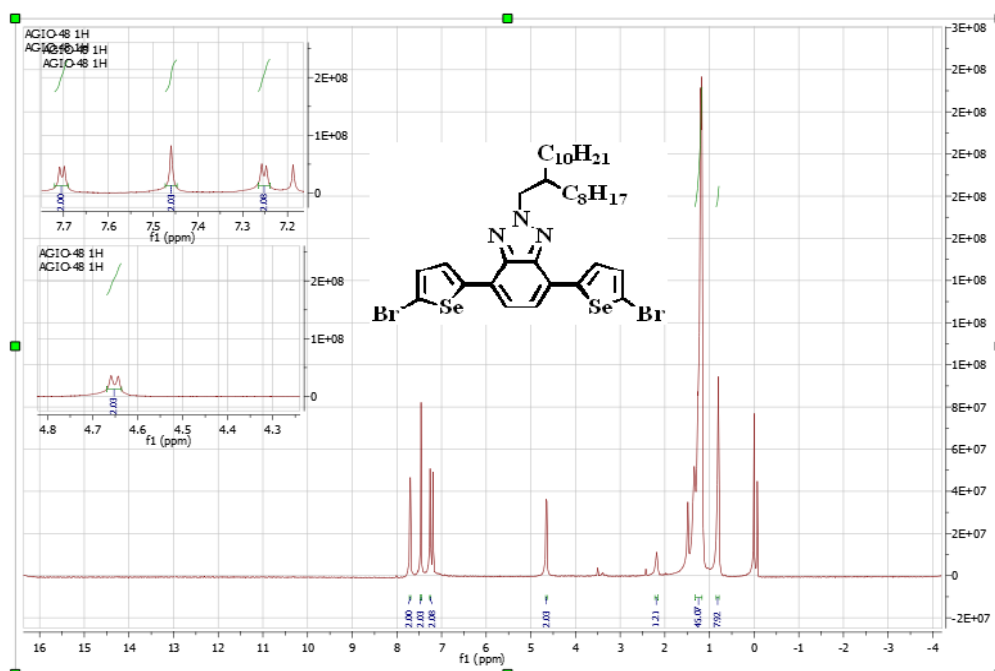


Figure 55. ^1H NMR of 4, 7-bis (5-bromoselenophen-2-yl)-2-(2-octyldodecyl)-2Hbenzo[d][1,2,3]triazole

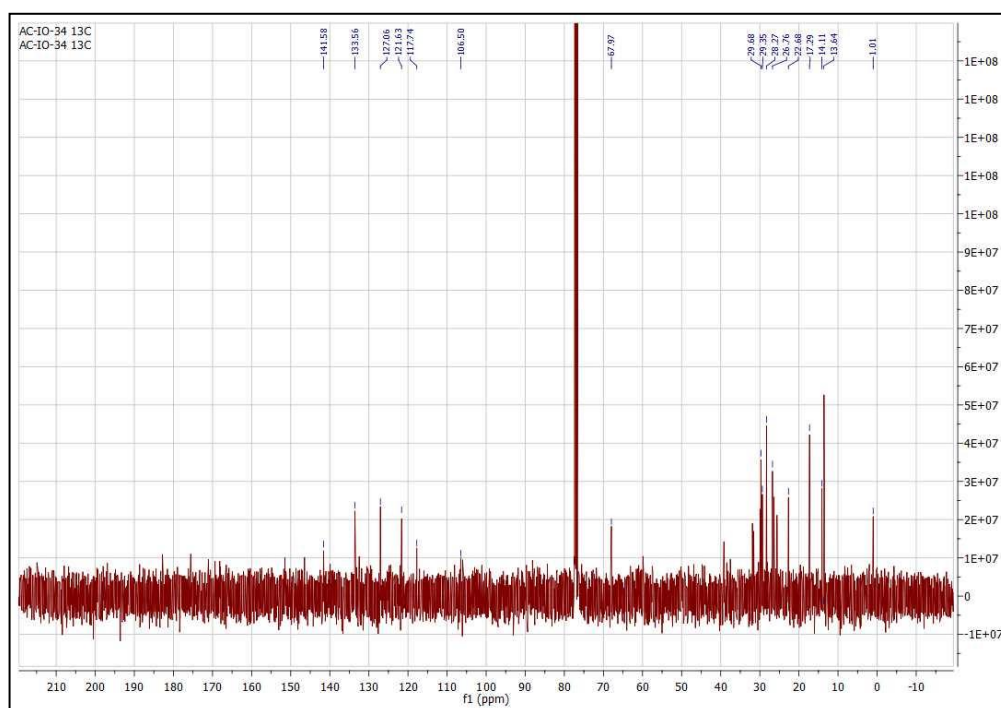


Figure 56. ^{13}C NMR of 4, 7-bis (5-bromoselenophen-2-yl)-2-(2-octyldodecyl)-2Hbenzo[d][1,2,3]triazole

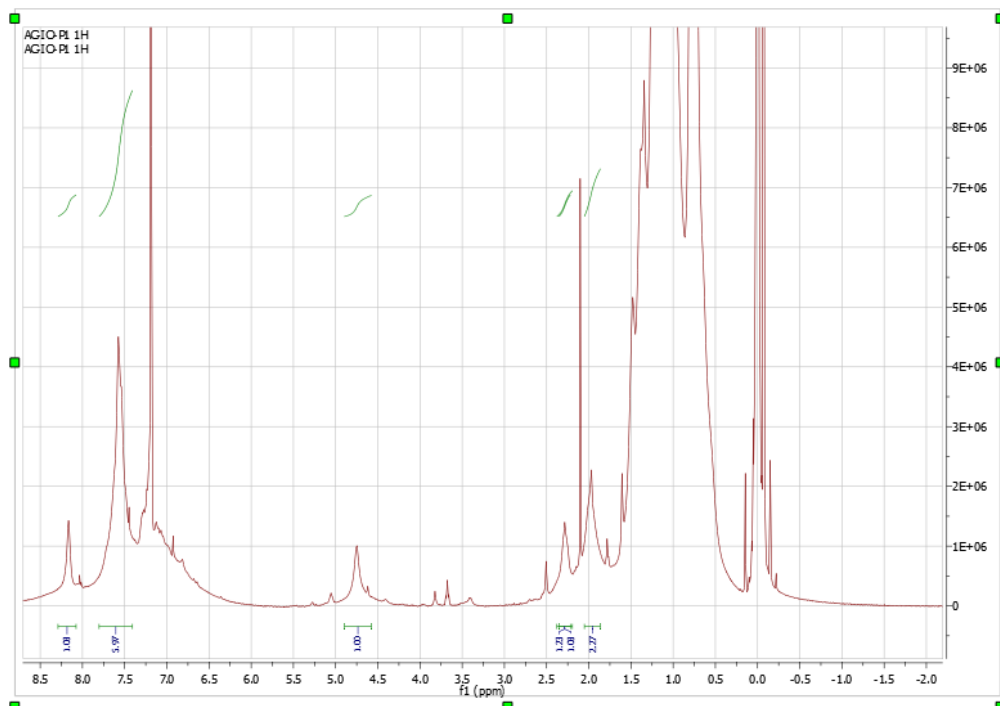


Figure 57. ^1H NMR of P1

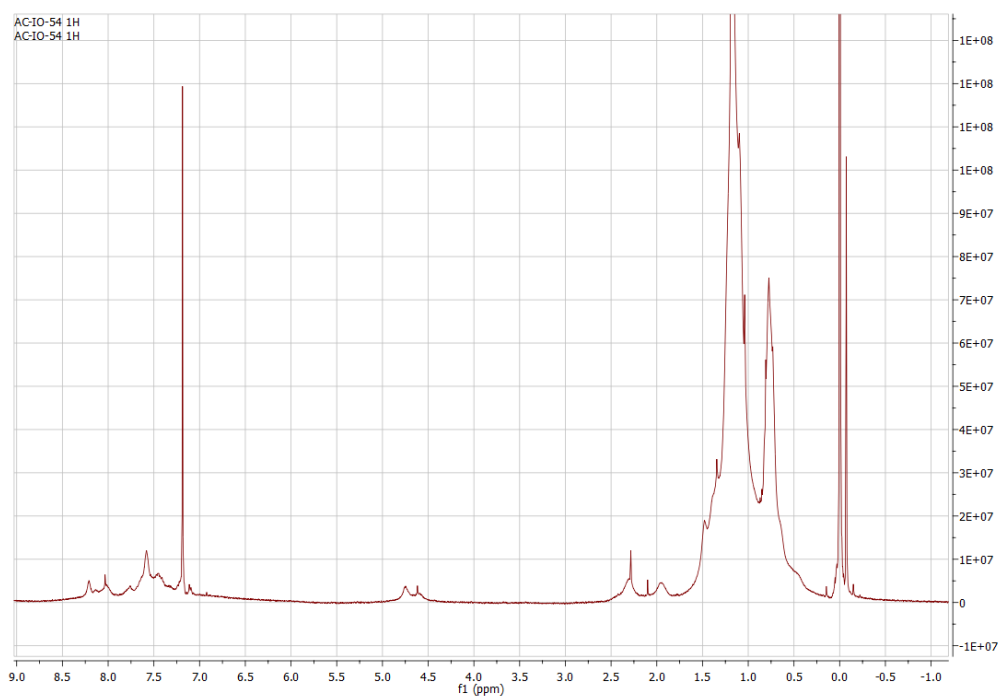


Figure 58. ^1H NMR of P2